CO4-1 Characterization of Additive in Lubricant using Small-Angle X-ray Scattering

Y. Oba, M. Hino[1], R. Motokawa, N. Adachi[2], Y. Todaka[2], R. Inoue[1], and M. Sugiyama[1]

Materials Sciences Research Center, Japan Atomic Energy Agency
[1]Institute for Integrated Radiation and Nuclear Science, Kyoto University
[2]Department of Mechanical Engineering, Graduate School of Engineering, Toyohashi University of Technlogy

INTRODUCTION: Lubricants usually contain a variety of additives to improve lubrication properties. In the lubricants, the additives form nanostructures such as micelles, which play a key role in lubrication properties. Small-angle scattering (SAS) is useful to characterize such nanostructures in solvent. However, SAS has been scarcely used in the field of tribology [1].

Therefore, we performed small-angle X-ray scattering (SAXS) measurements of the additives in the lubricants to determine proper experimental conditions and to obtain fundamental information needed for nanostructural analysis.

EXPERIMENTS: SAXS measurements were performed using the in-house SAXS instrument with Mo *K*α radiation. Scattering patterns were obtained using a two-dimensional detector (PILATUS 100k) equipped with a 1000 μm-thick silicon sensor. The path of X-ray between the entrance slit and up to the detector including the sample area was in vacuum to eliminate background scattering from air and vacuum windows. Oleic acid (OA) and oleyl acid phosphate (OLAP) were chosen as the additives. 1 mass% oleyl acid phosphate and 5 mass% oleic acid were dispersed in poly-α-olefin (PAO), respectively. The samples were sealed in sample cells made by stainless steel body, X-ray windows of cover glasses, and Viton O-rings. Two samples-to-detector distances (SDD), 0.4 and 1.8 m, were used to cover wide q range, where q is the magnitude of the scattering vector. The measurement times are 1 hour and 5 hours for 0.4 m and 1.8 m conditions, respectively.

RESULTS: Fig. 1 shows the SAXS profiles of 5 mass% OA in PAO, 1 mass% OLAP in PAO, and pure PAO. The scattering of an empty cell was subtracted as background. A peak is observed at around q = 4.5 nm^{-1} in all the samples including pure PAO. This reflects the nanostructure in pure PAO. The profiles of the 5 mass% OA in PAO are almost similar to those of pure PAO.

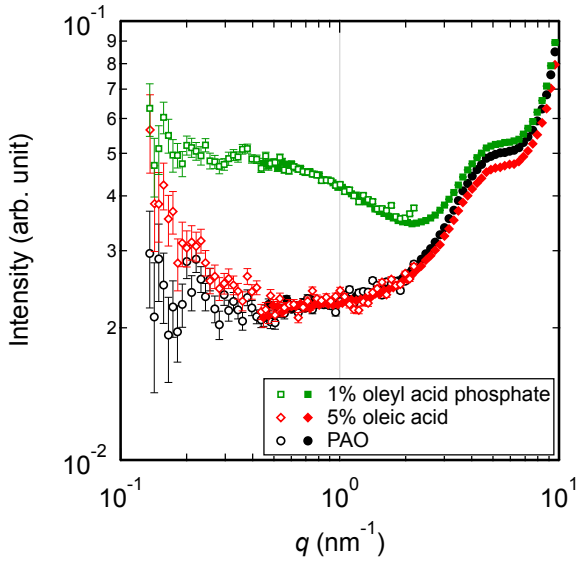

Fig. 1. SAXS profiles of 5 mass% OA in PAO, 1 mass% OLAP in PAO, and pure PAO. Open and filled symbols indicate the profiles obtained using SDD = 1.8 and 0.4 m, respectively.

Therefore, the scattering contrast of OA in PAO is probably too small to analyze. In contrast, 1 mass% OLAP in PAO shows a significant increase in the scattering intensity at q lower than about 2.5 nm^{-1}. This increase is the scattering of OLAP. The features of the scattering profiles are similar to the scattering profiles of tri-*n*-butyl phosphate in organic solvent [2]. This suggests that OLAP forms aggregate in PAO. In summary, we successfully observed the nanostructure of OLAP in PAO. For OA in PAO, denser sample is required to obtain reasonable scattering intensity.

ACKNOWLEDGMENTS: A part of this work was supported by JST "Collaborative Research Based on Industrial Demand" Grand Number JPMJSK1511, Japan.

REFERENCES:

[1] M. J. Covitch *et al.*, Adv. Chem. Eng. Sci., **5** (2015) 134-151.
[2] R. Motokawa *et al.*, J. Phys. Chem. B, **116** (2012) 1319-1327.

CO4-2 Synthesis of alloy nanoparticles in water solution by two steps reduction and one time γ-ray irradiation

F. Hori, Y. Uchimura, T. Yamada[1], T. Matsui[1], N. Taguchi[2], S. Tanaka[2] and Q. Xu[3]

Dept. of Engineering, Osaka Prefecture University

[1]*Center for Advanced Education of Entrepreneurship and Innovation, Osaka Prefecture University*

[2]*AIST, Kansai Center*

[3]*Institute for Integrated Radiation and Nuclear Science, Kyoto University*

INTRODUCTION: In general, it is known that metal nanoparticles (NPs) have some specific properties, which are not appeared in bulk materials such as catalytic activities, magnetic properties, electric conductivity and light absorption. These properties depend on its size, shape, structure, chemical composition and so on. They have many possibilities to applied for various industrial fields. However, it is not easy to fabricate multi elemental alloy NPs with controlling their size, shape and structure. Generally, many kinds of metal NPs commercially are synthesized by using chemical reaction method, which is not necessarily in water solution. Recent years, some reports show that it is possible to fabricate some metal NPs under irradiation reduction fields such as ultrasonic, solution plasma, electron beam, ion beam and gamma-ray [1]. We have been trying to synthesize various kinds of metal nanoparticles with size and shape controlled by gamma-ray irradiation reduction method. On the other hand, metal nanoparticles with high electronic conductivity is expected for the fields of printed electronics technologies as a metal nanoink. Cu is the high electronic conductivity and one of the most abundant resources on earth. However, the fabrication of Cu nanoparticle has a difficulty because its oxidation property. So far, we have successfully synthesized pure Cu nanoparticles in water by gamma-ray reduction method, but it was not stable. In this study, we have tried to synthesize Cu-Au alloy nanoparticles by two-step reduction with one gamma-ray irradiation.

EXPERIMENTS:

Aqueous solution with a given concentration of copper complex ($(CH_3COO)_2Cu{\cdot}H_2O$) with an additive of sodium dodecyl sulfate (SDS) and 8.5 vol% ethylene glycol was prepared. The solution was argon gas purged and sealed into polystyrene vessels. They were irradiated at about 300 K with 1.17 and 1.33 MeV gamma-rays from ^{60}Co radio active source at 4gamma irradiation facility in KURRI, Kyoto University. The total dose was fixed to 10 kGy with the dose rate of 1.0 kGy/h. After irradiation, a solution of 1.0 mM gold complex ($NaAuCl_4{\cdot}2H_2O$) was added with different ratios of Cu:Au=1:1, 4:1 and 9:1 in a nitrogen atmosphere. After irradiation, the samples were measured for UV–vis absorption spectra. The shapes and the structures for all colloidal products were observed by TEM (JEM-2000FX and FEI-Titan) and energy dispersive X-ray spectrometry (EDS). X-ray Photoelectron Spectroscopy (XPS) measurement at KEK-PF BL-27 and X-ray diffraction have also performed.

RESULTS:

Fig. 1 shows the light absorption spectra of each colloidal sample. After adding of the gold complex solutions, characteristic surface plasmonic absorption peaks of Cu and Au are observed. This result shows that gold ions are reduced in a Cu colloid fabricated by gamma-ray irradiation. Fig. 2 shows the XRD profiles for all samples. In this figure, it is confirmed that the formation of pure Cu, CuO, Au, Cu-Au compound and their solid solution. By analyzing of XPS results, it was found that reduced Cu ions have metalic combination in a particles. XRD result shows that after long period only in case of Cu:Au=9:1 pure Cu particles remains stable, but in another samples Cu and Cu alloys disappeared and only Au nanoparticles were survived.

REFERENCES:

[1] N.Taguchi *et al.*, Rad. Phys. Chem., **78** (2009) 1049-1053.

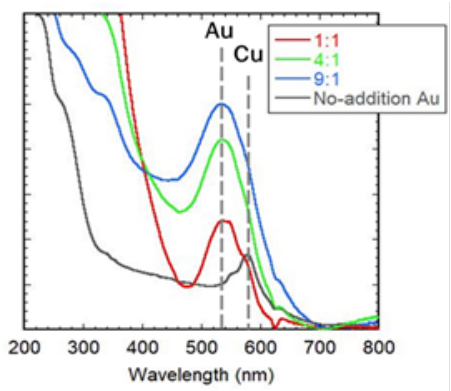

Fig.1. UV-vis spectra of gamma-ray irradiated samples.

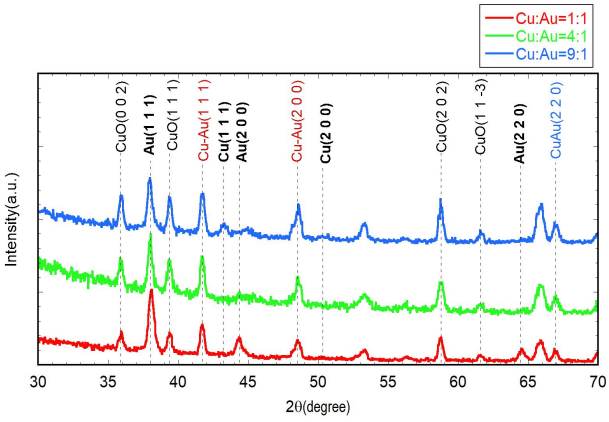

Fig. 2. XRD profiles of synthesized Au and Cu NPs by gamma-ray irradiation.

CO4-3 Defects structure and characterization of electron irradiated intermetallic alloys

F. Hori, N. Ogawa, A. Takano, K. Sugita, T. Yamada, K. Ohsawa[1], Q. Xu[2] and N. Abe[2]

Dept. of Quantum & Radiation Eng., Osaka Pref. Univ.
[1]*Res. Inst. of Appl. Mech., Kyushu University*
[2]*KURNS*

INTRODUCTION: In general, it is well known that intermetallic compounds has good properties such as specific strength to weight ratio, oxidation resistance and strength in elevated temperature. However, some of them arises degradation of fatigue strength caused by hydrogen embrittlement. The nature of their processes is not cleared yet. On the other hand, hydrogen is nowadays receiving a lot of attention for various kinds of materials research. It is important to clear the interaction between hydrogen and metallic materials for example hydrogen embrittlement, hydride formation and hydrogen induced transformation in hydrogen storage material. So far, we have been investigated the interaction between hydrogen atom and vacancies in B2 ordered intermetallic compounds. In that research, we found radiation induced hydrogen absorption by vacancies in B2 type of Fe-Al and Fe-Rh alloys. However, this effect is not confirmed for other type of intermetallic compounds. In this study, therefore, we have studied the interaction between hydrogen atom and vacancies in various type of intermetallic alloys, especially ZrCuAl intermetallic compound alloy.

EXPERIMENTS: Zr50%Cu40%Al10% alloy was prepared by arc melting method in argon gas atmosphere. Sliced samples with the thickness of 0.5 mm were annealed at 1073 K for 3 h. These specimens were irradiated with 8 MeV electron with water cooling system to the fluence of 1×10^{18} /cm^2 at KURRI, Kyoto University. Irradiation was carried out at about 330 K controlled. Cathodic charged hydrogen implantation have performed for before and after electron irradiated samples in a potassium hydroxide solution with a current of 2.621×10^{3} A/cm^2. All samples were measured by X-ray diffraction and positron annihilation Doppler broadening measurements. Thermal desorption spectroscopy (TDS) measurement have done for hydrogen implanted alloy samples annealing up to 600K with heating rate of 1 K/sec.

RESULTS: Figure 1 shows the XRD spectra of ZrCuAl alloy before irradiation, after electron irradiation and hydrogen charged after irradiation. In this alloy, irradiation induced phase transition and hydrogen induced new phase was not observed. Figure 2 shows the hydrogen desorption behavior from cathodic charged ZrCuAl alloys with and without electron irradiation. This figure clearly shows that hydrogen desorption behavior changes by electron irradiation. That is the desorption peak around 120 C disappeared and broad peak around 300–500 C appears instead. From these results, it found that metal hydride is not formed but hydrogen trapping by electron irradiation induced vacancies takes place.

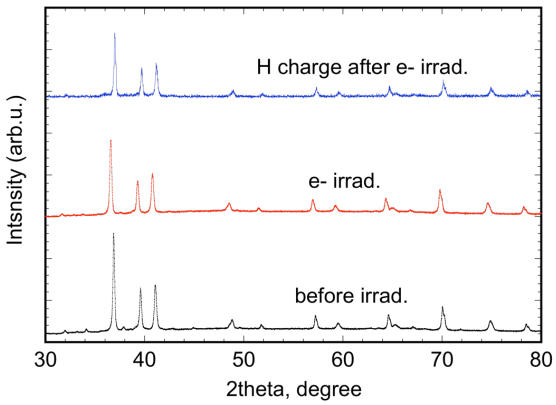

Fig. 1. XRD profiles of ZrCuAl alloy before irradiation, after electron irradiation and hydrogen charged after irradiation.

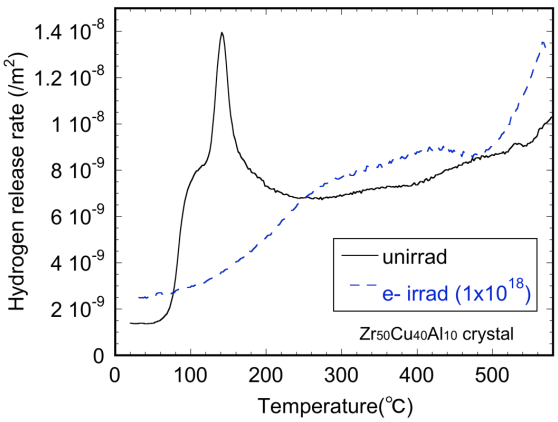

Fig. 2. TDS spectra of hydrogen desorption behavior for hydrogen charged ZrCuAl alloys with and without electron irradiation.

CO4-4 Magnetic Scattering Contribution in Iron Characterzed by Neutron Diffraction

Y. Oba, K. Mori[1], M. Hino[1] and R. Okumura[1]

Materials Sciences Research Center, Japan Atomic Energy Agency
[1]Institute for Integrated Radiation and Nuclear Science, Kyoto University

INTRODUCTION: Magnetic scattering contribution is one of the most unique features of neutron diffraction and thus widely used for the investigation of magnetic structures. However, it is scarcely used in the research and development of practical ferromagnetic materials, such as permanent magnets and soft magnetic materials. Since the magnetic scattering analysis can provide the information about the directions of magnetic moments, it would be useful to understand magnetization process, which is a key to achieve higher permeability in the soft magnetic materials [1]. Therefore, we carried out the neutron diffraction experiments of the soft magnetic materials to confirm that the magnetic scattering contribution can be observed in the magnetization process.

EXPERIMENTS: An iron rod (99.9%) with the diameter of 12.7 mm was selected as a typical soft magnetic material. The neutron diffraction experiments were performed using the Versatile compact neutron diffractometer (VCND) at the B-3 beam port of the Kyoto University Research Reactor (KUR) [2,3]. An electromagnet was placed on a sample goniometer to apply a magnetic field to the sample (Fig. 1). The maximum field is about 300 Oe.

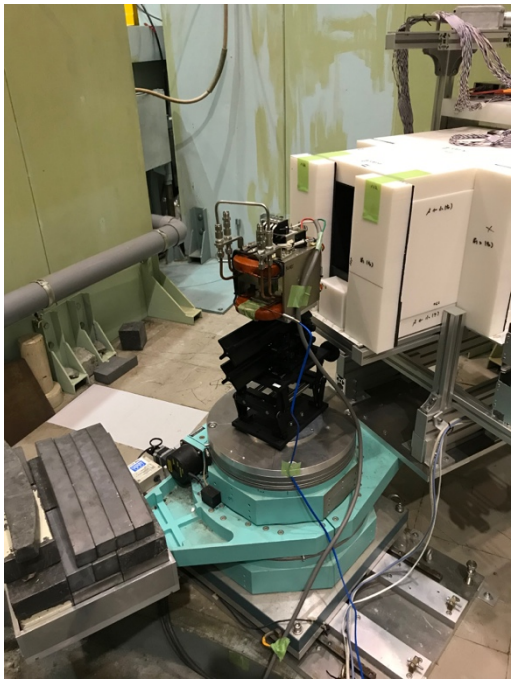

Fig. 1. Photograph of electromagnet installed at VCND. A magnetic field is vertically applied.

RESULTS: Fig. 2 shows the diffraction patterns of the iron rod and background. The iron rod shows clear Bragg peaks at 31º and 44º corresponding to (110) and (200) planes, respectively. Small peaks at 29º, 42º, and 50º come from the background caused by the electromagnet.

The diffraction pattern with a magnetic field is also shown in Fig. 2. The magnetic field was applied perpendicular to the scattering vector. In this condition, the magnetic scattering contribution must increase compared to a demagnetized state. The results indicate that the diffraction intensity with a magnetic field is higher than that without a magnetic field at the Bragg peaks, whereas the background intensity is not changed. This confirms that the magnetic scattering contribution can be observed in iron.

REFERENCES:

[1] M. Birsan *et al.*, Phys. Rev. B, **53** (1996) 6412-6417.
[2] K. Mori *et al.*, KURNS Prog. Rep. 2018, (2019) 128.
[3] K. Mori *et al.*, JPS Conf. Ser., (submitted).

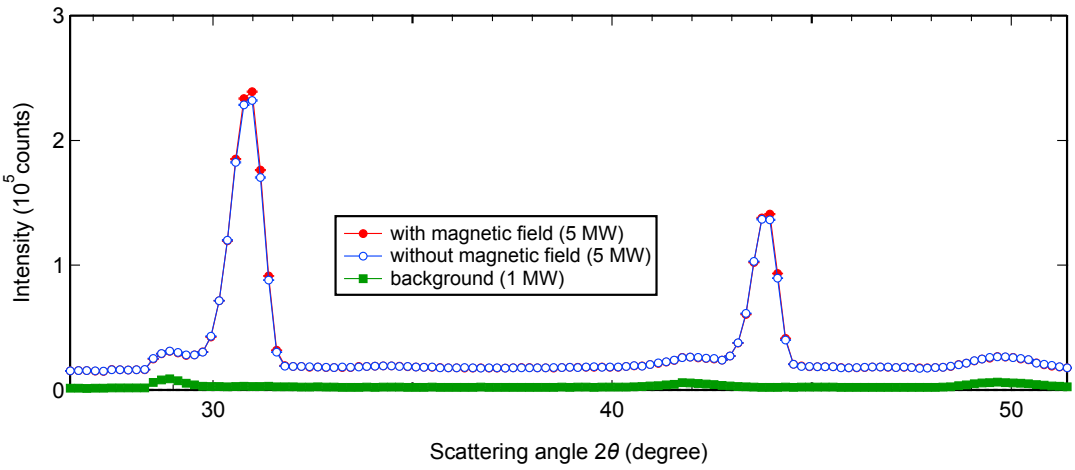

Fig. 2. Neutron diffraction patterns of iron and background. Filled and open circles denote the diffraction patterns of iron with and without a magnetic field, respectively. Filled squares is the diffraction patterns of background.

CO4-5 What Exists in a 2-nm-sized Molecular Caspule Assembeld in Water?

Y.-Y. Zhan[1], N. Sato, K. Morishima, M. Sugiyama and S. Hiraoka[1]

Institute for Integrated Radiation and Nuclear Science, Kyoto University
[1]Department of Basic Science, The University of Tokyo

INTRODUCTION: Molecular capsules and cages provide a confined nano-space in which sensing, stabilization, activation, reaction, and catalysis can be realized based on the selective encapsulation of target molecules in their cavity. Previously, we developed cube-shaped molecular capsules (nanocubes), which are assembled from six gear-shaped amphiphiles (GSAs) in water.[1] One of the nanocubes, **BM**, shows high thermal[1-3] and kinetic[4] stabilities, though the GSAs are not connected by strong chemical bonds but only mesh each other. The **BM** nanocube has a 1-nm-sized hydrophobic cavity, in which various neutral and anionic species are encapsulated.[1,3,5] The thermodynamic parameters for the encapsulation of anions in the nanocube were previously determined by ITC measurements, and the encapsulation is enthalpically favorable but entropically unfavorable. However, to correctly interpret the thermodynamic parameters, it should be clarified what exist(s) in the cavity of the nanocube before the encapsulation. Considering that the **BM** GSA is a dicationic molecule with Cl^- as counter anions, water molecules and/or Cl^- anion(s) would be trapped in the nanocube. In this research, SAXS measurements of the **BM** nanocube with and without NaCl were carried out, which enabled us to discuss what exist in the cavity of the nanocube.

EXPERIMENTS: SAXS profiles were measured with a laboratory SAXS instrument (Rigaku NANOPIX) installed at Institute for Integrated Radiation and Nuclear Science, Kyoto University. X-ray wavelength was 1.54 Å and the typical sample-to-detector distance was 350 and 95 mm. A sample of the nanocube was prepared by dissolving solid sample of **BM** GSA in Milli-Q water. The concentration of the nanocube was determined by UV spectroscopy before the SAXS measurements of the nanocube in pure water and in 100 mM NaCl aqueous solution.

RESULTS: The SAXS profiles and the Guinier plots for the BM nanocube in pure water and in 100 mM NaCl solution are shown in Figure 1. In our previous study of the SAXS measurements, two prominent peaks were observed for the nanocubes, which suggests that a discrete structure is formed in water and that the discussion on the precise structure of the nanocube is possible based on the position and the intensity of the peaks. It was found that a similar SAXS profile was observed irrespective of whether NaCl (100 mM) is added or not but that the radius of gyration (R_g) of the nanocube determined by the Guinier plot is largely affected by the salt. R_g of the nanocube in 100 mM NaCl is 7.3 ± 0.3 Å, while that in pure water is 9.6 ± 0.3 Å. As the peak positions of the SAXS profiles of the two are almost same, the change in the R_g values with and without NaCl would arise from the difference in the environment of the cavity of the nanocube not from change in the size of the nanocube. Indeed, the simulation of the SAXS profiles by changing the size or the shape of the nanocube caused the shift of the prominent peaks, and the SAXS profile of the nanocube in 100 mM aq. NaCl could not be well reproduced by simulation. These results strongly suggest that Cl^- anion(s) should be encapsulated in the nanocube in 100 mM aq. NaCl. In other words, the cavity of the nanocube in pure water should be filled with water molecules. Therefore, the encapsulation occurring in the **BM** nanocube can be described as the exchange of water molecules filled in the cavity with the guest molecule(s), so the release of unstabilized water molecules in the nanocube contributes to the encapsulation of anions.

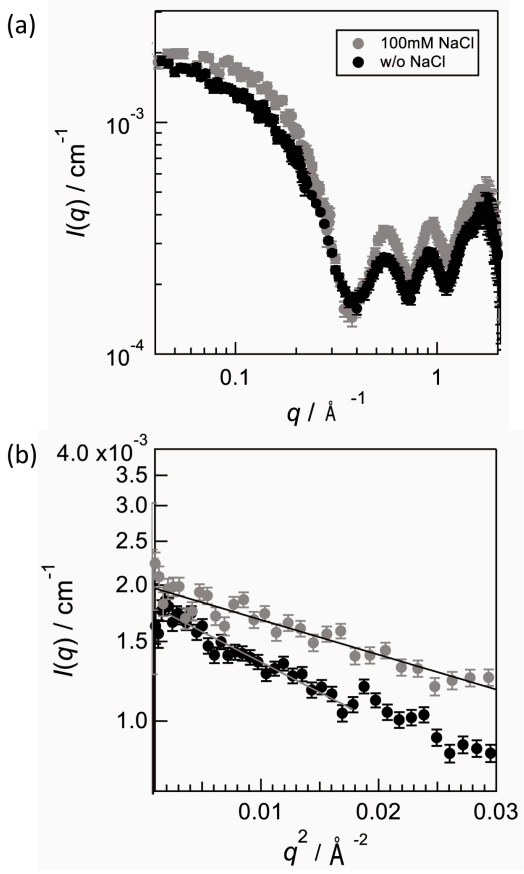

Fig. 1. (a) SAXS profiles of a solution of the **BM** nanocube in water with and without NaCl (100 mM). (b) The Guinier plots for the SAXS data.

REFERENCES:

[1] Y.-Y. Zhan *et al.*, *Commun. Chem.*, **1** (2018) 14.
[2] Y.-Y. Zhan *et al.*, *Chem. Eur. J.*, **24** (2019) 9130–9135.
[3] Y.-Y. Zhan *et al.*, *Nature Commun.*, **9** (2018) 4530.
[4] Y.-Y. Zhan *et al.*, *Nature Commun.*, **10** (2019) 1414.
[5] Y.-Y. Zhan *et al., Commun. Chem.*, **2** (2019) 107.

CO4-6 Damage Evolution in Neutron-irradiated Metals during Neutron Irradiation at Elevated Temperatures

I. Mukouda and Q. Xu[1]

Hiroshima International University
[1]Institute for Integrated Radiation and Nuclear Science, Kyoto University

INTRODUCTION: It is accumulated an attention that a damage structure in neutron irradiated metals differs if the temperature is varied during irradiation [1]. Especially effect of lower temperature irradiation on the development of damage structure in metals which are irradiated subsequently at higher temperature was reported to be remarkable because the point defects nucleate at lower temperature more frequently during an irradiation. Recently the temperature controlled irradiation devices were developed at KUR [2]. It becomes possible to irradiate continuously at two stage of temperature. In the present work, effects on damage formation in neutron-irradiated copper for the temperature variation were examined for an irradiation at low fluence regime.

EXPERIMENTS: Copper disks of 3mm in diameter were prepared with 99.999% nominal purity specimen. Before an irradiation, they were annealed for 5 hours at 1273 K in vacuum of 10^{-5} Pa. Specimens were irradiated by fission neutrons in a temperature controlled irradiation device in KUR-SSS. In the previous temperature varying irradiation, specimens were irradiated at first at 473K and 573K. After a radiation cooling, they were observed by electron microscopy. A TEM observation was carried out using g = (002) reflection with (g, 5g) condition for the specimens of (110) configuration. Voids were observed in a bright field image by taking a slightly under forcussed image. A triangular image was taken as stacking fault tetrahedra (SFT) and diffused dot image was tentatively taken to be an interstitial cluster.
Present temperature varying irradiation, specimens were irradiated at 473K-6hrs/573K-40hrs, 473K-23 hrs/573K-23 hrs and 473K-6 hrs/573K-20 hrs at 1MW. TEM observation are carried out recently.

RESULTS: In 473K-10hrs/573K-10hrs irradiation at 5MW, the number density of voids and SFT was smaller than those of constant temperature irradiation at 573K. Especially the decrease of number density of voids was significant [3]. shows dislocations in the specimen. Dislocations were not decorated by interstitial clusters. The number density of SFT was smaller than the value in copper which were irradiated at constant temperature of 573 K. Only one void was observed in specimens as in this picture, which means the formation of voids was suppressed significantly by the present temperature elevation irradiation.
Neutron-irradiated copper at 573K for 10 hours at 5MW, the dislocation structure show no decorated interstitial clusters around dislocation. Interstitial clusters, which were accumulated along dislocation lines, were unified to grow to dislocations. This makes development of complicated structure of dislocations as reported by Mukouda and Shimomura [4].
The suppression of void formation in temperature-varied irradiation suggests that the nucleation of voids during a constant temperature irradiation at 573K in copper occurs during the period of dislocation decoration by interstitial clusters.
In 473K-6hrs/573K-40hrs irradiation at 1MW, the number density of voids and SFT was significant smaller than those of constant temperature irradiation at 573K as shown in Fig. 1. Only one void were observed. TEM observation of other irradiation condition specimens are progress at the present.

REFERENCES:
[1] N. Yoshida, Q. Xu, H. Watanabe, Y. Miyamoto and T. Muroga, J. Nucl. Mater., 212-215 (1994) 471.
[2] T. Yoshiie, Annual Reports of KUR (1998).
[3] I. Mukouda and Q. Xu, KURNS progress report 2018, Co4-7.
[4] I. Mukouda and Y. Shimomura, Material Science & Engineering A309-310 (2001) 190-197.

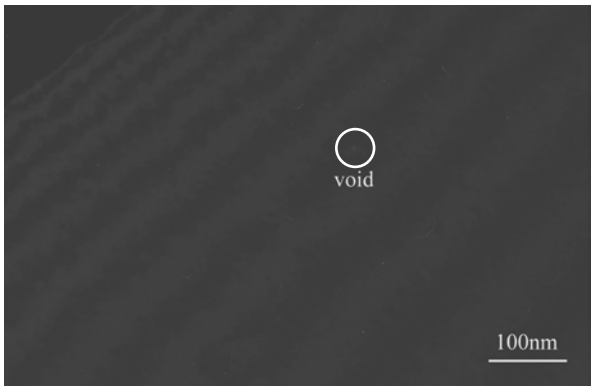

Fig. 1. Damages observed in neutron-irradiated copper with temperature varying schedule. The irradiation was carried out at first at 473K for 6 hours and subsequently at 573 K for 40 hours at 1MW.

CO4-7 Radiation Resistivity of Ferrite Permanent Magnets Against Neutrons

Y. Iwashita[1], M. Abe[1], T. Yako[1], T. Kurihara[2], M. Fukuda[2], M. Sato[2], T. Sugimura[2], Y. Iinuma[3], Y. Fuwa[4], Y. Kuriyama[3] and K. Takamiya[3]

[1]*Institute for Chemical Research, Kyoto University*
[2]*Accelerator Laboratory, KEK*
[3]*Institute for Integrated Radiation and Nuclear Science, Kyoto University*
[4]*J-PARC Center, JAEA*

INTRODUCTION: Permanent magnets are used as material of beam optical elements. While rare earth magnets, such as NeFeB and SmCo, are known to have radiation demagnetization [1], there is not enough information for ferrite magnets, which are economical but have less remanent field strength. In order to verify the resistivity of ferrite magnets, we carried out a trial experiment on radiation demagnetization of ferrite magnets irradiated by neutrons at Kyoto University Research Reactor (KUR).

EXPERIMENTS: We acquired cylindrical anisotropic ferrite magnets with 5 mm diameter and 2 mm length that have easy-axis parallel to the cylinder axis. They are popular off-the-shelf Y30H (Strontium Ferrite magnets). Since they seemed to have common non-uniformity on the easy-axis and they were randomly magnetized, they were re-magnetized to have better magnetic uniformity. We measured their magnetic field at both end surfaces with a Tesla meter (SENIS 3MH3) using a magnet fixture jig prepared for this experiment. The jig has a 0.5 mm thick plastic plate between the Hall probe and the magnet end surface to avoid a direct contact between them. Since the Hall probe measurement is sensitive to the positioning error of magnets, another measurement method was developed. This rotates the small magnet in a coil and the amplitude of the induced voltage is taken. This method is less sensitive to the positioning error.
The irradiation times were 46 hours at 1 MW operation and 6 hours at 5 MW operation (HYD), and 4 weeks (Long Term). In these two irradiation conditions, estimated values of thermal neutron fluence on the samples are 5.7×10^{18} [n/cm^2] and 8.6×10^{18} [n/cm^2], respectively. A permanent magnet samples packed in aluminum sheets was placed into a capsule together and sent to the reactor. After the residual radioactivity of the magnet and capsule decayed sufficiently, we took out the magnet samples from the capsule and measured the magnetic field. We compared the magnetic field strength before and after the irradiations.

RESULTS: Fig. 1 shows the ratios of the magnetic field strength before and after the irradiation. The error bars show the standard deviations of measured data for each magnet.
The broken vertical green line in Fig. 1 denotes neutron dose at which radiation demagnetization becomes significant for NeFeB magnets [1]. Ferrite magnets were found to be more resistant to the radiation than NeFeB magnets. According to the data taken so far, the characteristic radiation demagnetization dose is estimated about 1.4×10^{20} [n/cm^2]. Because of the regression function form, the data points at less radiations have almost no effect on the fitting result. The magnetization will be degraded to half at dose of about 1×10^{20} [n/cm^2].

PERSPECTIVES: The radiation hardness level of ferrite magnets close to those for SmCo magnets is an important information for communities handling radiations. The ferrite magnets would be widely used in such applications.
More irradiation dose with improved magnetic field measurement procedure clarified the demagnetization as a function of the dose level. Measurements on other magnets such as NdFeB and SmCo magnets with the same procedure is planned for a systematic understanding on the radiation demagnetization on practical magnet materials.

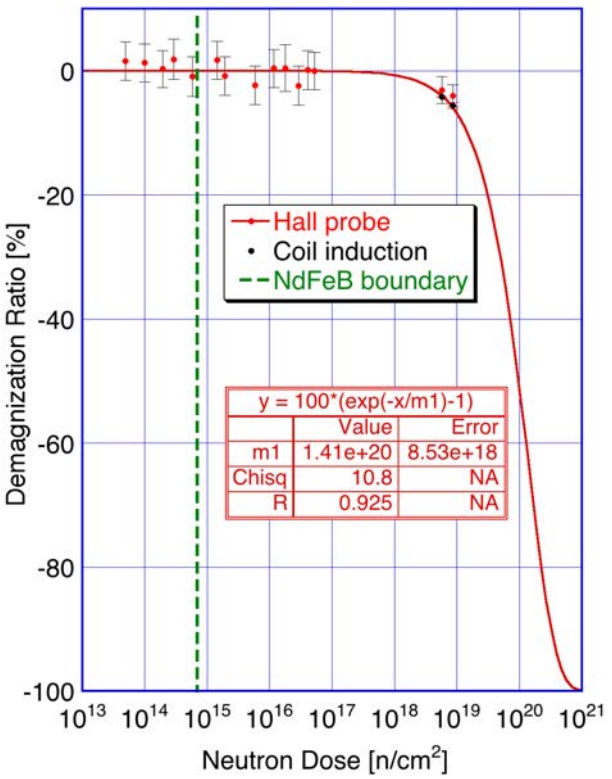

Fig. 1: Ratio of radiation demagnetization of ferrite permanent magnet.

REFERENCES:

[1] X. -M. Marechal, T. Bizen, Y. Asano, H. Kitamura, Proceedings of EPAC, Edinburgh, Scotland, 2006.

CO4-8 Elucidation of the Mechanism of the Screw-sense Induction of Polymer Backbone Based on the Small Angle X-ray Scattering and Dynamic Light Scattering Measurements

Y. Nagata[1], M. Suginome[2], M. Sugiyama[3], R. Inoue[3], N. Sato[3], and K. Morishima[3]

[1] *Institute for Chemical Reaction Design and Discovery, Hokkaido University*
[2] *Graduate School of Engendering, Kyoto University*
[3] *Institute for Integrated Radiation and Nuclear Science, Kyoto University*

INTRODUCTION: Increasing attention has focused on the structural control of helical polymers owing to their potential applications for asymmetric catalysts, chiral stationary phase, and chiroptical materials. Recently, we found that single-handed helical poly(quinoxaline-2,3-diyl)s (PQXs) bearing chiral side chains exhibit a solvent-dependent helix inversion,[1-3] which can serve as effective scaffold for chirality-switchable materials. [4-7] To elucidate the mechanism of the helix inversion of PQXs, we have investigated the detailed structures of a PQX (100mer) with right- or left-handed structures in tetrahydrofran-d_8 (THF-d_8) or a mixed solvent of 1,1,2-trichloroethane-d_3 (1,1,2-TCE-d_3) and THF-d_8 (4/1, v/v) by using small-angle neutron scattering (SANS) experiments, in conjunction with theoretical calculations.[8] The obtained structures of the PQX suggested that the right-handed structure in THF-d_8 is well solvated, while the left-handed structure in 1,1,2-TCE-d_3/ THF-d_8 (4/1, v/v) is less solvated.

Our recent interest has focused on the impact of the dynamics of the side chains on the screw-sense induction. So far, we have carried out quasielastic neutron scattering (QENS) measurements to elucidate the impact of the molecular dynamics on the solvent-dependent helix inversion of the PQX at BL-02 DNA in J-PARC. In this study, we have carried out dynamic light scattering (DLS) measurements for the detailed analysis of the results of the QENS measurements.

EXPERIMENTS: A PQX bearing (*R*)-2-octyloxymethyl side chains (100mer) was prepared according to our previous paper. The light scattering measurements were carried out with a 22-mW He-Ne laser, an Avalanche Photo Diode (APD, ALV, Germany) mounted on static/dynamic compact goniometer, ALV/LSE-5003 electronics, and ALV-5000 Correlator (ALV-Laser Vertriebsgesellschaft GmbH, Langen, Germany). The measurements were performed at 313 K and CONTIN analysis was used to obtain the probability of decay rate at each *Q*.

RESULTS: The PQX was dissolved in THF-d_8 or a mixed solvent of 1,1,2-trichloroethane-d_3 (1,1,2-TCE-d_3) and THF-d_8 (4/1, v/v), respectively, to carry out DLS measurements (Fig 1). In the both cases, the decay constant Γ and the square of the wave vector q^2 showed linear relationship, affording the diffusion constants in these solvents. We are now working on the analysis of the QENS measurements by using the results of the DLS measurements.

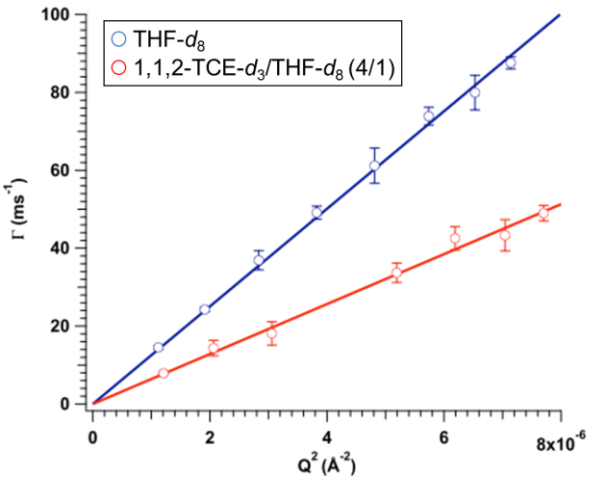

Fig. 1 Correlation between the decay constant Γ and the square of the wave vector q^2. The measurements were carried out using solutions of the PQX in THF-d_8 (blue) or a mixed solvent of 1,1,2-trichloroethane-d_3 (1,1,2-TCE-d_3) and THF-d_8 (4/1, v/v, red).

REFERENCES:

(1) Yamada, T.; Nagata, Y.; Suginome, M. *Chem. Commun.* **2010**, *46*, 4914-4916.
(2) Nagata, Y.; Yamada, T.; Adachi, T.; Akai, Y.; Yamamoto, T.; Suginome, M. *J. Am. Chem. Soc.* **2013**, *135*, 10104-10113.
(3) Nagata, Y.; Nishikawa, T.; Suginome, M. *J. Am. Chem. Soc.* **2015**, *137*, 4070-4073.
(4) Nagata, Y.; Nishikawa, T.; Suginome, M. *Chem. Commun.* **2012**, *48*, 11193-11195.
(5) Nagata, Y.; Takagi, K.; Suginome, M. *J. Am. Chem. Soc.* **2014**, *136*, 9858-9861.
(6)Nagata, Y.; Uno, M.; Suginome, M. *Angew. Chem. Int. Ed.* **2016**, *55*, , 7126-7130.
(7) Nishikawa, T.; Nagata, Y.; Suginome, M. *ACS Macro Lett.* **2017**, *6*, 431-435.
(8) Nagata, Y.; Nishikawa, T.; Suginome, M.; Sato, S.; Sugiyama, M.; Porcar, L.; Martel, A.; Inoue, R.; Sato, N. *J. Am. Chem. Soc.* **2018**, *140*, 2722-2726.

Crystal structure analysis of Abalone shell

K. Iwase and K. Mori[1]

Department of Materials Science and Engineering, Ibaraki University

[1]Institute for Integrated Radiation and Nuclear Science, Kyoto University

INTRODUCTION: Biomineralization, the process through which living organisms form mineralized tissues such as shell, bone, pearl, eggshell, exoskeleton, usually takes place at ambient temperature and pressure. The formed biominerals, nanocomposites made of inorganic and organic substances,[1,2] are renowned for their mechanical properties[3]. For example, the shell of Strombusgigas is formed of 99% of volume inorganic phase calcium carbonate with the aragonite structure and 1% of organic phase. The nacre in this shell is 3000 times tougher than single crystals of the pure mineral and has a "crossed lamellar microarchitecture"[4,5]. Calcium car-bonate has three polymorphs: aragonite, calcite, and va-terite. Calcite is the thermodynamically most stable phase of calcium carbonate at ambient conditions, whereas aragonite and vaterite are less stable. The calcite phase is rhombohedral with space group $R\bar{3}c$, the aragonite phase is orthorhombic with the Pnma space group, and the va-terite phase has the $P6_3/mmc$ space group.

In this study, we investigated the inner, and outer layers of Abalone shell (AWABI) by neutron diffraction

EXPERIMENTS: NPD data were collected by using the step-scan mode of a diffractometer (B-3) with 1.0294 Å wavelength. The powdered sample was sieved to a particle size of < 20 μm for the NPD measurements. The Abalone shell was measured as non-powder sample.

RESULTS: Fig. 1 shows neutron diffraction profiles of synthesized aragonite, synthesized calcite and Abalone shell (AWABI). The shell has two layers. The inner layer and outer layer are aragonite structure and calcite structure, respectively. The peak broadening was observed in aragonite and calcite of the Abalone shell.

Fig. 2 shows the Rietveld refinement of the Abalone shell. The shell consists of 82 mass % aragonite and 18 mass % calcite. The refined lattice parameters of aragonite phase of the Abalone shell were a = 0.5667(8) nm, b = 0.4962(6) nm and c = 0.791 (1) nm, respectively. On the other hand, the refined lattice parameters of synthe-sized aragonite were a = 0.5736(4) nm, b = 0.4961(3) nm and c = 0.7960 (5) nm. The aragonite phase of the Aba-lone shell expanded anisotropically along a and c axes from the synthesized aragonite. The calcite phase of the Abalone shell indicated lattice parameters a = 0.490(1) nm and c = 1.712(8) nm, which is smaller than that of the synthesized calcite, a = 0.4988(3) nm and c = 1.705(1) nm.

The lattice parameters of the Abalone shell are different from the synthesized sample. The Abalone shell has the anisotropic lattice strain both aragonite and calcite phases.

The mechanical properties of Abalone shell is superior to single crystals of the pure mineral [4,5], which may be relate to the anisotropic lattice expansion.

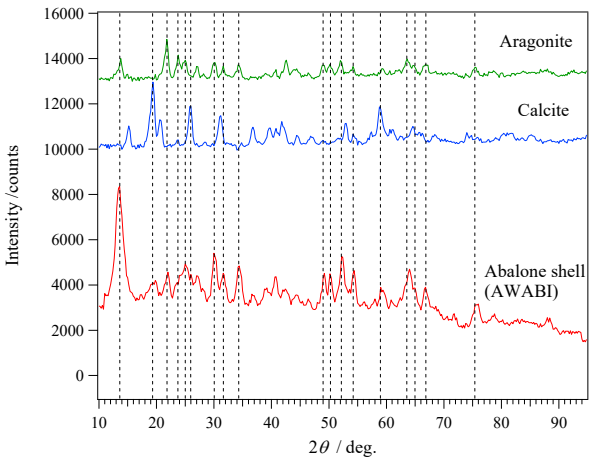

Fig. 1 Neutron diffraction profiles of synthesized aragonite, synthesized calcite and Abalone shell.

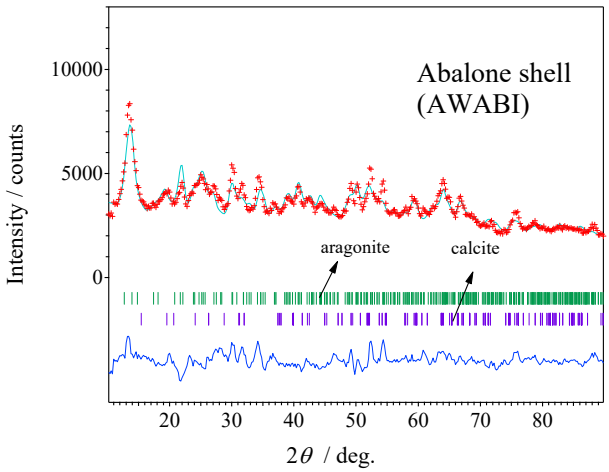

Fig. 2. Rietveld refinement pattern of Abalone shell.

REFERENCES:

[1] Y. Dauphin, Curr. Opin. Colloid Interface Sci., **7** (2002) 133-138.
[2] Y. Dauphin, *et al*., J. Struct. Biol., **142** (2003) 72-280.
[3] A. P. Jackson, *et al*., Proc. R. Soc. London, B **234** (1988) 415-440.
[4] S. Kamat, *et al.*, Nature **405** (2000) 1036-1040.
[5] B. L. Smith, *et al.*, Nature **399** (1999) 761-763.

CO4-10 Radiochemical Research for the Advancement of $^{99}Mo/^{99m}Tc$ Generator by (n, γ) Method (2)

Y. Fujita, M. Seki, Y. Namekawa, K. Nishikata, K. Kato, N. Sayato, K. Tsuchiya, T. Sano[1], Y. Fujihara[2], J. Hori[2], H. Yoshinaga[2]. J. Zhang[2], T. Suzuki[3] and H. Suematsu[3]

Department of JMTR, Japan Atomic Energy Agency
[1] Atomic Energy Research Institute, Kindai University
[2]Institute for Integrated Radiation and Nuclear Science, Kyoto University
[3]Graduate School of Engineering, Nagaoka University of Technology

INTRODUCTION: The research and development (R&D) has been carried out for the production of Molybdenum-99 (^{99}Mo) by the neutron activation method ((n, γ) method) from viewpoints of limited availability of high-enriched uranium, no-proliferation and nuclear security, and disposal of nuclear fissile materials. It is essential to improve the properties of Alumina (Al_2O_3) used widely as Mo adsorbent for the $^{99}Mo/^{99m}Tc$ generator.

In last year's study, four types of Al_2O_3 specimens were prepared and their properties were evaluated by batch adsorption (Static adsorption) which immersed Al_2O_3 specimens in the sodium molybdate solution (Mo solution). In this study, Mo was adsorbed by column adsorption (Dynamic adsorption) which packed Al_2O_3 specimens in a tube and flown Mo solution in that. Then the elution test of Tc-99m was carried out.

EXPERIMENTS: The MoO_3 pellets were fabricated by the cold pressing and sintering method. Density of MoO_3 pellets was about 60%T.D. The MoO_3 pellet pieces (about 1.5g) were irradiated in the Pn-2 of the KUR for 20min. After the irradiation, the irradiated MoO_3 pellet pieces were dis-solved with 6M-NaOH solution. Then, the Mo adsorption tests of the Al_2O_3 specimens were carried out with the Mo solution (10mg-Mo/mL, pH4) at RT. A column was prepared by packing 1g of each Al_2O_3 specimens into a PFA tube (I.D. 1.59mm). ^{99}Mo was adsorbed by flowing in the column a Mo solution (0.3~0.4mL/min) using a peristaltic pump. After this process, the saline was flowed through in this column about every 24h and the ^{99m}Tc was eluted from each Al_2O_3 specimens. The activities of ^{99}Mo and ^{99m}Tc in the solution were measured by the γ-ray spectrometer.

RESULTS: Table 1 shows the comparison results of ^{99}Mo adsorption capacity by each Al_2O_3 specimen in dynamic adsorption and static adsorption. In dynamic adsorption, the Mo adsorption capacity was decreased as compared with that by the static adsorption. It seems that packing the Al_2O_3 specimens into an elongated tube improved the washing efficiency and removed Mo weakly adsorbed on the Al_2O_3 specimens, remaining in the column.

Table 2 shows the elution rate of ^{99m}Tc from the Al_2O_3 specimens, the pH of the ^{99m}Tc eluate and the $^{99}Mo/^{99m}Tc$ ratio, which is an indicator of the ^{99}Mo contamination rate in the ^{99m}Tc eluate, on the first milking. As a result, the elution rate of ^{99m}Tc was over 100% at 1.5mL of milking in dynamic adsorption, while the elution rate was around 56-87% in static adsorption. It is thought that the elution efficiency was improved by filling Al_2O_3 specimens into a long and thin tube, whereby the contact between saline and Al_2O_3 specimens became uniform. The pH of the eluted ^{99m}Tc solution didn't depend on the method of adsorbing Mo, and satisfied the standard value of pH 4.5-7.0. This suggests that Al_2O_3 specimens was sufficiently cleaned by either method. The $^{99}Mo/^{99m}Tc$ ratio was greatly reduced in dynamic adsorption compared to that by static adsorption. Therefore, the $^{99}Mo/^{99m}Tc$ ratio is greatly affected by the method of adsorbing Mo, which means the column shape and the linear flow rate during elution may affect that.

In the future, the effects of column diameter and linear flow rate on ^{99m}Tc elution and ^{99}Mo desorption will be investigated.

Table 1 Results of ^{99}Mo adsorption capacity of Al_2O_3 specimens

Items		^{99}Mo adsorption capacity (mg/g-Al_2O_3)
Specimen-1 (D-201-300)	Dynamic	51.9
	Static	57.4
Specimen-2 (V-V-300)	Dynamic	48.7
	Static	55.4
Specimen-3 (V-B-300)	Dynamic	63.8
	Static	88.8
Specimen-4 (Medical)	Dynamic	27.0
	Static	39.0

Table 2 ^{99m}Tc elution rates from Al_2O_3 specimens and the pH, the ^{99}Mo contamination of ^{99m}Tc solution in 1st milking

Items		^{99m}Tc elution rates at 1.5mL in Milking (%)	pH of ^{99m}Tc solution*	^{99}Mo contamination at 1.5mL in Milking [$^{99}Mo/^{99m}Tc$ (%)]
Specimen-1 (D-201-300)	Dynamic	104.2	4.86	0.080
	Static	56.8	5.06	0.58
Specimen-2 (V-V-300)	Dynamic	105.4	4.77	0.500
	Static	79.5	4.50	3.46
Specimen-3 (V-B-300)	Dynamic	110.0	5.21	0.132
	Static	68.4	4.69	2.69
Specimen-4 (Medical)	Dynamic	108.0	4.48	1.108
	Static	86.6	4.41	8.77

* in 4.5mL (Dynamic), in 9.0mL (Static)

REFERENCES:

[1] Y. Suzuki *et al.*, Transactions of the Materials Research Society of Japan, **43** (2018) 75-8.

CO4-11 Radiophotoluminescence phenomenon in Cu-doped silica glasses prepared from porous silica glass

Y. Takada, R. Hashikawa, Y. Nishi, A. Kinomura[1], T. Saito[1], A. Okada[2], T. Wakasugi[2], K. Kadono[2]

Graduate School of Science and Technology, Kyoto Institute of Technology
[1]Institute for Integrated Radiation and Nuclear Science, Kyoto University
[2]Faculty of Materials Science and Engineering, Kyoto Institute of Technology.

INTRODUCTION: Radiophotoluminescence (RPL) is a luminescence phenomenon in a material induced by exposure to high-energy radiation. Silver-activated phosphate glasses are well known as a material exhibiting the RPL phenomenon, and these glasses are applied for a personal dosimeter [1]. However, only a few materials have been found to have a prominent RPL other than the silver-activated phosphate glasses. Thus, extensive exploration is performed to obtain materials having high performance RPL behavior. We have reported that in aluminoborosilicate glasses doped with an extremely low content of copper, intense photoluminescence is induced by the exposure of the glasses to X-ray and γ-ray irradiation [2]. The mechanism of the RPL phenomenon for the Cu-doped glass is considered to be as follows [2]:
Copper in the glass mainly exists as divalent Cu^{2+} or monovalent Cu^{+} ions. The former, Cu^{2+} ion, has no luminescence while the latter, Cu^{+} ion, has a bright one around 500 nm by the excitation at 240 nm. When the glass doped with copper is exposed to high-energy radiation, electron and hole pairs are generated in the glass as expressed by (1) and a part of them are captured by Cu^{2+} and Cu^{+} ions, respectively as equations, (2) and (3).

$$\text{Glass} \rightarrow h^{+} + e^{-} \quad (1)$$
$$Cu^{2+} + e^{-} \rightarrow Cu^{+} \quad (2)$$
$$Cu^{+} + h^{+} \rightarrow Cu^{2+} \quad (3)$$

When the electron capture process (2) is more predominant than the hole capture process (3), the concentration of the luminescence species, Cu^{+}, increases and as a result, the luminescence will increase.

We have investigated the RPL behaviors of copper in other glass systems. Here, we report the photoluminescence behaviors of Cu-doped silica glass that was prepared through the immersion of a porous silica glass in a $Cu(NO_3)_2$ aqueous solution using the glass as a starting material [3].

EXPERIMENTS: The porous silica glass used as a starting material was prepared from a phase-separated borosilicate glass with a composition, $9.0Na_2O \cdot 26.6B_2O_3 \cdot 64.4SiO_2$. The porous silica glass was immersed in 0.0005 to 0.005 M $Cu(NO_3)_2$ aqueous solution to dope copper into the porous silica glass. The Cu-doped porous silica glass was sintered at 900°C for 2 hours, and cut and optically polished to 1 mm thickness. The Cu-doped silica glass (abbreviated as Cu-SG, hereafter) was exposed to γ-ray or X-ray radiations. The γ-ray irradiation experiments were performed with ^{60}Co γ-ray at the Co-60 Gamma-ray Irradiation Facility at Institute for Integrated Radiation and Nuclear Science, Kyoto University. The irradiation dose was represented as absorbed dose for water. The X-ray irradiation was performed using an X-ray source with a Rh target.

RESULTS: Figure 1 shows the photoluminescence spectra of the 0.0005 M-Cu-SG silica glass (prepared by the immersion in 0.0005 M $Cu(NO_3)_2$ solution) measured before and after the γ-ray irradiation with the intensity of approximately 800 Gy and the appearance of the glass under the UV-radiation. The spectra and the appearance of the 0.005 mol% Cu-doped aluminoborosilicate glass (abbreviated as Cu-ABS25) was also shown for comparison. Both spectra after the irradiation are normalized with the intensity of the spectra before the irradiation, respectively. The photoluminescence intensity for the Cu-SG increased approximately two times by the irradiation (see the solid line arrow) while that for the Cu-ABS25 increased four times (dotted line arrow). The spectrum of the Cu-SG shifted to the longer wavelength direction after the irradiation and the color of the luminescence varied from blue to yellow. This is due to the difference in the coordination environment of the Cu^{+} generated by the electron capture from that of the Cu^{+} existing before the irradiation as the glass prepared.

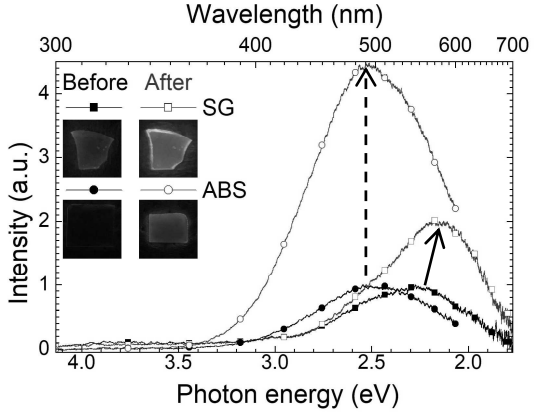

Fig. 1. Emission spectra of Cu-doped glasses (Cu-SG and Cu-ABS). The spectra were normalized with the peak intensities of the spectra before irradiation.

The intensity of photoluminescence after the irradiation was proportionally increased with the absorbed dose. The ratio of the intensities after and before the irradiation decreased with the concentration of copper incorporated into the glass.

REFERENCES:

[1] R. Yokota, *et al.*, *J. Phys. Soc. Jpn.*, **23** (1966) 1038-1048.

[2] H. Hashikawa, *et al.*, *J. Am. Cer. Soc.*, **102**(4) (2019) 1642-1651.

[3] D. Chen, *et al., Appl. Phys. Lett.*, **86** (2005) 231908.

CO4-12 Study of resonant frequency change with irradiation dose of piezoelectric PZT element

M . Kobayashi, T . Miyachi , S . Takechi[1], Y. Morita[1], A. Umehara[2], Reo Kunimatsu[2] and Ryo Sasaki[2]

Planetary Exploration Research Center, Chiba Institute of Technology
[1]Graduate School of Engineering, Osaka City University
[2]Department of Engineering, Osaka City University

INTRODUCTION: In the previous years, we have found that when irradiating high intensity heavy ions to a piezoelectric element (400 MeV/n Xe beam at HIMAC of the National Institute of Radiological Sciences [1][2]), its resonance frequency and anti-resonance frequency are shifted and also the impedance at the resonance frequency and anti-resonance frequency are changed by beam irradiation and then the electromechanical coupling coefficients of those piezoelectric elements were decreased.

There are two types of radiation damage to general materials, due to ionizing and non-ionizing dose effects (or displacement damage). Since the piezoelectric element is a crystalline material, it is considered that the crystal is damaged by the beam irradiation and thus the characteristic parameter such as the resonance frequency has changed. However, detailed mechanism such as its mechanism is not known.

Therefore, in this study, we investigated the response of the piezoelectricity against energetic electron beam irradiation which has dominantly ionizing effect (less non-ionizing effect) to compare with the previous results.

EXPERIMENTS AND RESUTLS: In this year, we had two experiment campaigns for electron beam irradiation to piezoelectric PZT elements in KURRI-LINAC.

(1) The first experiment on May 27 to 31 in 2019: In the experiments up to the previous year, we found that the decrease in piezoelectricity due to electron irradiation was smaller than that due to xenon irradiation. Therefore, we devised an experiment setup to improve the quality of the experiment in order to have more quantitative discussion. The setup of irradiation target holder and positioning mechanism has been improved for more precise positioning against the electron beam because results were sometimes varied even if the beam condition was the same. As the results, the change of the electromechanical coupling coefficients of irradiated PZT targets against the current of electron beam became less variable.

We have monitored the temperature on the surface of the target piezoelectric elements which were cooled by forced air cooling during electron irradiation to the elements because the piezoelectricity can be lost or reduced by heat when the temperature becomes close to its Curie point. We estimated the internal temperature of the target piezoelectric elements with a thermal analysis taking into account of the forced air cooling and noticed that the internal temperature can be higher than the surface one. We performed how the piezoelectricity is reduced by temperature by using a thermostatic chamber and obtained a function of “piezoelectricity loss” of the piezoelectric element as temperature.

(2) *The second experiment on January 27 to 31 in 2020*: We performed the second electron irradiation experiment so that the internal temperature may not become over the point at which the piezoelectricity begins to be reduced, by monitoring the surface temperature of the target ones.

As the results, we could measure the net reduction in piezoelectricity due to electron beam irradiation. An experiment was conducted in which one specimen was irradiated with an electron beam for 15 hours or more, which we had never done previously because it was difficult to ensure the reproducibility of the experiment before this experiment.

We confirmed that the electromechanical coupling coefficient changes in the experiment of electron beam intensity, which is considered to be the effect of radiation only. For more better measurement, we used the other cable to connect the target piezoelectric with the measurement devices of impedance analyzer to exclude the effect of the capacitance of the cable and then we found that the measurement results vary depending on the cable attached to measure the piezoelectricity of the piezoelectric element. We will improve the situation in the future.

In this experiment campaign, we measured gamma rays emitted from radio-activated target piezoelectric material. That radioactivity may be produced by neutrons created by energetic electron. In order to determine the net effect of electron irradiation, we will evaluate the effect of radiation damage by neutron by analyzing the gamma ray spectra that we obtained in the experiments.

SUMMARY AND FUTURE PROSPECTS: In the experiments up to the previous year, we had difficulty to ensure reproducibility such as the alignment of the target with respect to the electron beam, but we were able to establish an experimental setup for high-precision measurement. As a result, we were able to specify a certain temperature point distinguish only the effects of radiation irradiation to piezoelectricity decrease. There is a problem with the cable for measurement, but we will solve the problem for experiments in the next experiment campaign for more further accurate measurements.

REFERENCES:

[1] M. Kobayashi *et al.*, Japanese Journal of Applied Physics 53, 066602 (2014).
[2] M. Kobayashi *et al.*, Japanese Journal of Applied Physics 52, 126604 (2013).

CO4-13 Formation of radiation defects on tungsten and their influence on effect of hydrogen isotope retention

K. Tokunaga, M. Matsuyama[1], M. Hasegawa, K. Nakamura and Q. Xu[2]

Research Institute for Applied Mechanics, Khushu University
[1]Hydrogen Isotope Research Center, University of Toyama
[2]Institute for Integrated Radiation and Nuclear Science, Kyoto University

INTRODUCTION: It is of a great importance to clarify phenomena of implantation, retention, diffusion and permeation of tritium (T) on surface of the armor materials of the first wall/blanket and the divertor on fusion device from a viewpoint of precise control of fuel particles, reduction of tritium inventory and safe waste management of materials contaminated with tritium. Refractory metals such as tungsten (W) is potential candidate for the armor of the first wall and the divertor plate of the fusion reactor because of its low erosion yield and good thermal properties. The armor material will be subjected to heavy thermal loads in the steady state or transient mode combined with high energy neutron irradiation that will cause serious material degradation. In addition, high energy runaway electrons would bombard the armor materials along the equatorial plane in fusion device. It is considered that these cause radiation damage and enhance tritium retention. In the present works, T exposure experiments have been carried out on W samples which were irradiated by high energy electrons to investigate effects of high energy electrons irradiation on microstructure and tritium retention of W. In this fiscal year, pure W and recrystallized W were irradiated by high energy electron beam. Before and after that, positron annihilation experiment was carried out to identify the radiation defect. In addition, EBSD（Electron Back Scatter Diffraction Patterns）analyses has been carried out on the specimens before and after the electrons irradiation. Tritium exposure experiments have been carried out using a tritium (T) exposure device.

EXPERIMENTS: W samples used were ITER specification W (ALMT-grade) (SR-W) and its recrystallized W (RC-W). The SR-W was fabricated via a powder metallurgical route including cold isostatic pressing, sintering, hot rolling, and heat treating to relieve the residual stresses. Some of the machined SR specimens were subjected to a full recrystallization treatment at 2000 ºC for 1 hr in vacuum. Sizes of the specimens were 10 mm x 10 mm x 1mm (10 mm x 10 mm : ND-TD). The surface of the both samples were polished to be mirrored. High energy electrons irradiation has been carried out using LINAC in Institute for Integrated Radiation and Nuclear Science, Kyoto University. An peak energy of electron irradiated was 8 MeV and DPA was 5.8 x 10^{-3}. Temperature during the irradiation was measured by thermocouples which was contacted with a backside of the W samples. Before and after that, positron annihilation experiment was carried out to identify the radiation defect. In addi-tion, EBSD（Electron Back Scatter Diffraction Patterns）analyses has been carried out on the specimens before and after the electrons irradiation. T exposure experiments have been carried out using a T exposure device in University of Toyama. Pressure of the T gas was 1.3 kPa and T exposure was kept for 4 h. T concentration in the gas was about 5 %. Temperatures of pre-heating and T exposures were 100 ºC and 100 ºC. After the exposure to T gas, T amount retained in surface layers of the sample was evaluated by β-ray-induced X-ray spectrometry (BIXS) and imaging plate (IP) measurements.

RESULTS: As shown in Fig. 1, mean lifetime from RC-W is smaller than that from SR-W. After the e irradiation, mean lifetime of both increases. τ_1 and τ_2 from the SR-W is bigger than that from RC-W. In addition, I_2 from RC-W is bigger than that from SR-W. Because τ_2 of RC-W after the e irradiation is 266.1 ps, defects are considered to aggregate by temperature increase due to the irradiation.

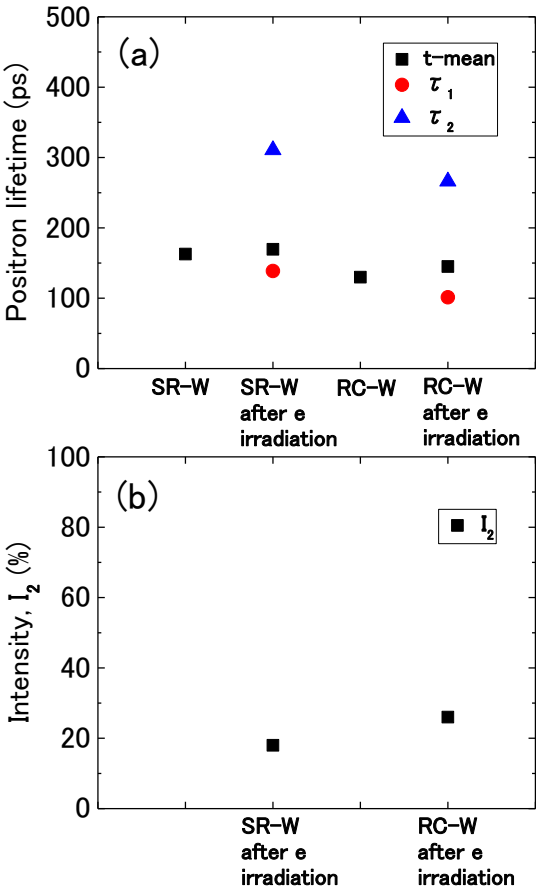

Fig. 1. Positron life time(a) and intensity of I_2 (b).

Tritium release behavior from neutron-irradiated FLiNaBe

K. Katayama, K. Kubo, K. Tsukahara, A. Ipponsugi, M. Oya, T. Takeishi[1], S. Fukada, and Y. Iinuma[2]

Department of Advanced Energy Engineering Science, Kyushu University
[1]Faculty of Engineering, Kyushu University
[2]Institute for Integrated Radiation and Nuclear Science, Kyoto University

INTRODUCTION: FLiNaBe, which is a mixed molten salt of LiF+NaF+BeF_2, is a promising liquid blanket material for a fusion reactor [1]. Tritium is produced in FLiNaBe by the nuclear reaction between neutrons and Li in the blanket. In the self-cooling system where the tritium breeding material itself transport heat to the heat exchanger, FLiNaBe plays two important roles of tritium transport and heat transport. Since FLiNaBe have a low solubility for hydrogen isotopes, the generated tritium tends to release from FLiNaBe. This property means that tritium can be easily recovered from FLiNaBe but also a part of tritium is lost to the outside of cooling tubes by the permeation on the way to the tritium recovery system. In order to control tritium safely and to design tritium recovery system, it is necessary to understand the fundamental behavior of tritium generated inside FLiNaBe by nuclear rection. In this study, the solid state sample of FLiNaBe was irradiated by thermal neutrons at Kyoto University Research Reactor, and tritium release behavior from the free surface of FLiNaBe by heating was observed in Kyushu University.

EXPERIMENTS: In the powders of LiF, NaF and BeF_2 were mixed in a Ni crucible under Ar atmosphere. The Ni crucible was put in the stainless-steel heating pot and repeatedly heated to 500 ℃ with Ar purging to remove impurity water vapor. The heating was repeated to homogenize the FLiNaBe. The prepared sample of FLiNaBe was packed into polyethylene bag with Ar gas and it was installed into a capsule. The thermal neutrons irradiation was performed by at pneumatic tube 2 (Pn-2) in Kyoto University Research Reactor with the fluence of at Pneumatic Tube 2 (Pn-2) of the 1.7×10^{15} cm^{-2}.

Tritium release experiment was carried out in Kyushu University. The schematic illustration of experimental apparatus is shown in Fig.1 The irradiated sample was put in a Mo crucible and it was installed in the stainless-steel reaction tube. The sample was heated to 600 ℃ with Ar purge. The chemical form of tritium released from the sample was expected to be TF and HT (T_2) and HTO (T_2O). In this experiment, since HT and T_2, HTO and T_2O cannot be distinguished, here these are represented as HT and HTO, respectively. HTO was collected in a cold trap, which was a spiral cupper tube immersed in ethanol with dry ice. TF was collected in a first water bubbler, and HT were collected in a second water bubbler after conversion to HTO by a CuO bed. The water of each bubbler was sampled periodically to observe the changes with time in release rates of TF and HT. After the experiment was finished, the temperature was increased to room temperature and cumulative HTO in the cold trap was purged by Ar and it was collected in a new water bubbler.

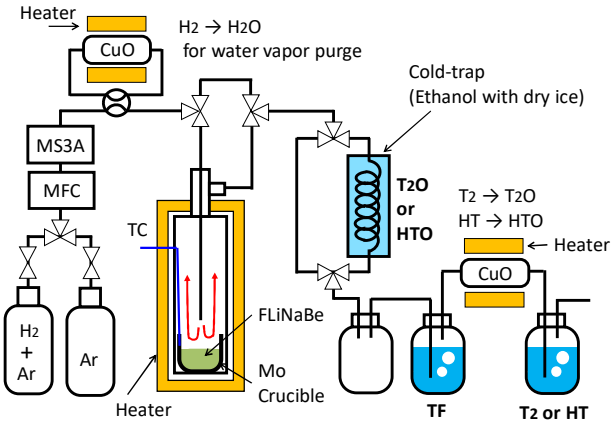

Fig.1. The schematic of experimental apparatus.

RESULTS: Fig.1 shows cumulative HT and TF released from neutron irradiated FLiNaBe in the initial heating to 600 ℃. As shown in Fig.1, most tritium was released as HT. After cooling the temperature below the melting point, the heating at 700 ° C was performed again. As a result, the release rate of TF gradually increased, and the rates of TF and HT reached the same degree. Initially tritium would be presence as TF in FLiNaBe but after melting TF was considered to react with Mo on the crucible and Fe on the reaction tube and converted to T_2. It can be said that as the fluoridation on the metal surface progressed, the reduction reaction of TF decreased, and the release rate of TF increased. This result suggests the possibility of redox control of TF by Mo. The release ratio of each chemical form was approximately TF: HT: HTO = 30:64:6. The majority of tritium was released as HT (or T_2). This result indicates that corrosion of metals by TF occurred in tritium release process. In the next experiment, the effect of H_2 purge on the suppression of corrosion will be investigated.

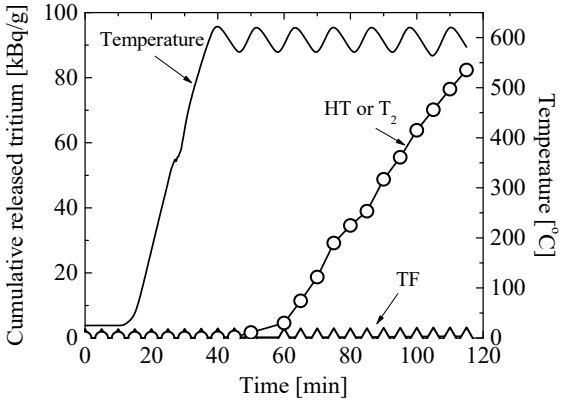

Fig.2. HT, T_2 and TF release from irradiated FLiNaBe.

CO4-15 Positron Age-Momentum Correlation Mesurements of γ-rays Irradited Polystyrene

H. Tsuchida[1,2], S. Konishi[2], Q. Xu[3]

[1]*Quantum Science and Engineering Center, Kyoto University*
[2]*Department of Nuclear Engineering, Kyoto University*
[3]*Institute of Integrated Radiation and Nuclear Science, Kyoto University*

INTRODUCTION: Studies on the irradiation-induced damage in polymers are of technical importance for developing radiation-resistance materials. In this work, we investigate microstructure changes of free volume in polystyrene induced by γ-rays irradiation at high dose. The free volume affects materials properties. The resultant damage was analyzed by the age-momentum correlation (AMOC) positron annihilation technique. The AMOC is a correlated measurement of the positron lifetime (positron age) and the momentum of the annihilating positron-electron pair. We study the radiation-induced dame near free volume of polystyrene via the annihilation processes of ortho-positronium (o-Ps).

EXPERIMENTS: The experiments were performed at the Co-60 γ-rays irradiation facility of KURNS. Polystyrene was used as a target specimen. The specimens with a thickness of 2-mm were irradiated with Co-60 γ-rays with energies of 1.17 and 1.33 MeV at various doses of 30, 200, 300 and 400 kGy. The irradiation experiments were performed at room temperature. The dose rate was 10 kGy/h. In the specimens after irradiation, we analyzed the resultant damage using β^+–γ based AMOC measurement system with Ge-68 positron source.

RESULTS: Based on the observed AMOC spectrum, we obtained variation of S parameter as a function of positron age (t), where S corresponds to the positron annihilation Doppler Broadening, which is defined as the ratio of the counts in the central position of the annihilation photopeak to the total counts in the peak. Figure 1 shows typical results. In this figure, S parameter at time region t = 0–3 ns corresponds to annihilation of free positrons or para-positronium (p-Ps). S at t > 3 ns corresponds to the pick-off annihilation of o-Ps formed in the free volume of polystyrene. The behavior strongly depends on the radiation dose, and the S parameter significantly decreases with increasing dose.

The S parameter of o-Ps is attributed to interactions of o-Ps with low-momentum electrons near free volume. We defined an average value of S parameter at time region 3 ns < t < 7 ns as the S parameter for o-Ps pick-off annihilation. Figure 2 shows its dose dependence. One can see that the S parameter decreases with increasing γ-rays radiation dose. In this case, the measured lifetime of o-Ps annihilation (τ_3 = 2.03 ns) remains unchanged after irradiation. We found that radiation damage near free volume increases linearly with dose, and there is a clear correlation between the S parameter and γ-rays radiation dose.

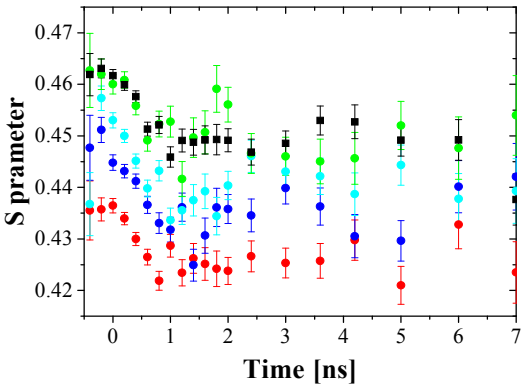

Fig. 1. Time dependent S-parameter of the o-Ps pick-off annihilation for before irradiation (■) and after Co-60 γ-rays irradiation at different dose: 30 kGy (●), 200 kGy (●), 300 kGy (●), and 400 kGy (●).

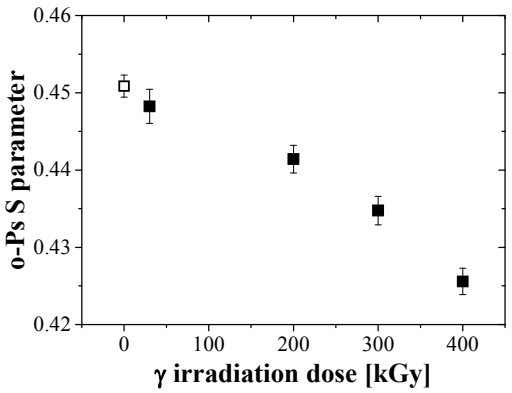

Fig. 2 Variation of S parameter for the o-Ps pick-off annihilation as a function of dose. The symbols denote data observed for before (□) and irradiated specimens (■).

CO4-16 Formation of nano-structures on Ge surfaces by ion irradiation and study on its formation mechanisms

J. Yanagisawa, R. Tsukamoto[1], K. Ishihara, Q. Xu[2], A. Yabuuchi[2], K. Takamiya[2] and A. Kinomura[2]

School of Engineering, The University of Shiga Prefecture

[1]*Graduate School of Engineering, The University of Shiga Prefecture*

[2]*Institute for Integrated Radiation and Nuclear Science, Kyoto University*

INTRODUCTION: We have reported that the formation of swelled nano-porous structures can be formed on Ge surfaces by Ga, Au or Si ion irradiations at the energy of 100-200 keV, but no such structures were observed by 15-30 keV ion irradiations [1]. We have also observed the formation of nano structures on the 25-60 keV Ar^+-irradiated areas of the Ge (110) surfaces, and the measurements of S parameters from the Doppler broadening of annihilation gamma-rays as a function of incident positron energy by the KUR slow positron bean system were performed [2]. The increases of the S parameters were observed for the ion-irradiated surfaces by the 25-50 keV Ar^+ with the ion fluences of 1-5 x 10^{16} cm^{-2}, showing the formation of atomic vacancies and/or voids on the ion-irradiated surfaces. On the other hand, we have found that nano-scale bumps on both Si and SiO_2 surfaces were formed by Ga^+ irradiation at an energy of 0.5 or 4 keV. In the present study, such Ga^+ irradiation was performed on Ge (110) surfaces and the S parameter was measured.

EXPERIMENTS: Ga^+ ion irradiation on the Ge (110) chip surfaces (each size of 1.5 x 1.5 cm^2) was performed using a needle type liquid-metal ion source at the acceleration voltage of 0.5 or 4 kV with the ion fluence of 1 x 10^{14} or 10^{15} cm^{-2}. S parameters were measured using the KUR slow positron beam system.

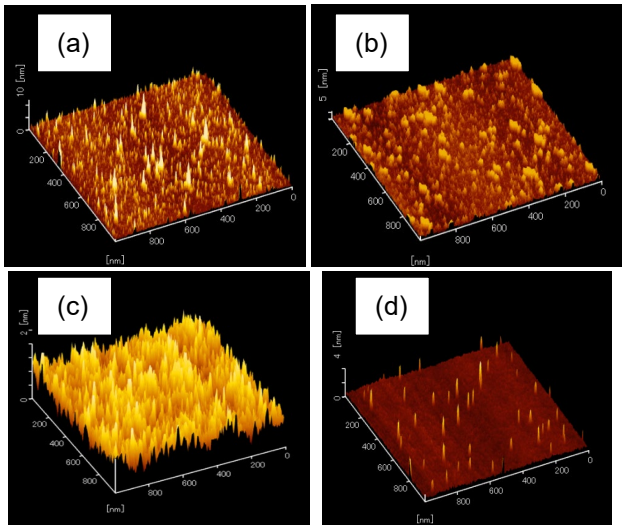

Fig. 1. AFM images of Ga^+-irradiated (using ion energy and fluence of (a) 0.5 keV and 1x10^{14} cm^{-2}, (b) 0.5 keV and 1x10^{15} cm^{-2}, (c) 4 keV, 1x10^{15} cm^{-2}, respectively,) and (d) un-irradiated Ge(110) surfaces.

RESULTS and DISCUSSION: Figure 1 shows the three-dimensional atomic force microscope (AFM) images of the Ga^+-irradiated surfaces. Figure 2 shows the S parameters as a function of positron energy for the corresponding samples as shown in Fig. 1. It is found that the behavior of the S parameter for the 0.5 keV, 1 x 10^{14} cm^{-2} Ar^+ irradiated surface was almost the same as that for the un-irradiated surface, although the values were unnaturally different each other. This can be supported from the similar AFM images, as shown in Figs. 1(a) and 1(d), although the density of the bumps was different. For the larger Ar^+ fluence and irradiation energy, however, the surface morphology was drastically changed, as shown in Figs. 1(b) and 1(c). This might be relevant to the drastic increase in the S parameters for them.

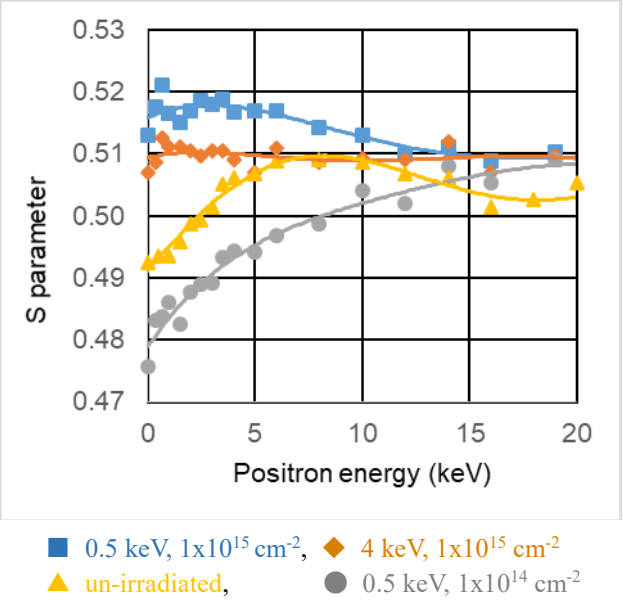

Fig. 2. S parameters for low-energy Ga^+-irradiated and un-irradiated Ge(110) surfaces as a function of positron energy.

CONCLUSION: Effect of the low-energy Ga ion irradiation on Ge (110) surfaces was studied using S parameters of the slow positron beam measurements. It is found that Ga^+ irradiation at lower energy (such as 0.5 keV) and lower fluence (1 x 10^{14} cm^{-2}) makes almost no effect on the formation of atomic vacancies and/or voids on the Ge surfaces.

REFERENCES:

[1] J. Yanagisawa, K. Takarabe, K. Ogushi, K. Gamo and Y. Akasaka, J. Phys.: Condens. Matter **19** (2007) 445002 (10pp).

[2] J. Yanagisawa, Q. Xu, A. Yabuuchi, K. Takamiya, and A. Kinomura, KURNS Progress Report 2018 (Kyoto University), CO4-9 (30037).

CO4-17 Evaluation of Structural Vacancies in Icosahedral Cluster Solids using Positron Annihilation

J. Takahashi[2], R. Nakajima[3], K. Kitahara[1], A. Yabuuchi[3], N. Oshima[4], I. Kanazawa[2], A. Kinomura[3], K. Kimura[1]

[1]Department of Advanced Materials Science, The University of Tokyo
[2]Department of Physics, Tokyo Gakugei University
[3]Institute for Integrated Radiation and Nuclear Science, Kyoto University
[4]National Institute of Advanced Industrial Science and Technology (AIST)

INTRODUCTION:

The thermodynamically stable Al-based icosahedral quasicrystals, which contain transition metals, have the anomalous electrical-conductivities, such as semiconductor-like properties [1]. However, there is no evidence for a gap as in semiconductors, and the structure is highly orderd, although it is no periodic. Mayon et al.[2] proposed a possible explanation for the unusual transport properties of Al-based quasicrystals in terms of hopping processed between wave functions mainly localized inside icosahedral clusters. Kimura et al.[3] have discussed the importance of vacant centers of the icosahedral clusters in the anomalous transport properties and stabilities of Al-based quasicrystals. They have shown that 12-atoms Al icosahedra with a vacant center have a covalent bonding nature, while 13-atoms with a center atom have a metallic bonding nature. Kirihara et al.[4] performed an electron density distribution analysis for 1/1 AlReSi approximant crystal and 1/0 AlRe approximant crystal by the MEM/Rietvelt method, which induced metallic-covalent bonding conversion in Al-based quasicrystals and approximant crystals. Positron annihilation method is powerful one for detecting structural vacancies of icosahedral quasicrystals[5]. Recently Kimura and coworkers [6] have done positron annihilation measurements of the positron lifetime, coincidence Doppler broadening(CDB), and depth profiling by slow positron beams for 1/1 AlReSi approximant crystals. They showed that 1/1 AlReSi approximant crystal has structural vacancies in the order of 10^{-3}, which are identified to be center sites of the first shell of icosahedral clusters, and then found that the structural vacancy density of metallic 1/1 AlReSi with less Re is lower than that of non-metallic AlReSi with more Re. These results accelate further investigation of the relationship between structure, bonding nature, and electrical properties for 1/1 AlReSi approximant crystals with different Re concentrations, leading to better understanding of physics behind quasicrystals and approximant crystals in terms of the proposed metallic-covalent binding conversion which occurs according to the occupation and vacany of the center sites of the Al icosahedral clusters. Tamura et al.[7] have measured the electrical-conductivities of AlPdRu quasicrystals, 2/1 AlPdRu approximant crystal, and 1/0 AlPdRu approximant crystal. They found very interesting resuls. That is, quasicrystal AlPdRu and 2/1 AlPdRu approximant crystal have non-metallic properties, while 1/0 AlPdRu approximant crystal have metallic properties. It is of significance to investigate AlPdRu quasicrystal and, AlPdRu approximant crystals, from the standpoint of structural vacancy density. In this study, we have measured the Doppler broadening of quasicrystal AlPdRu, 2/1 approximant crystal AlPdRu, and 1/0 approximant crystal AlPdRu by the slow positron beam, and also measured coincidence Doppler broadening(CDB) of 2/1 approximant crystal AlPdRu and 1/0 approximant crystal AlPdRu.

EXPERIMENTS and RESULTS:

By using the slow positron beam, we have estimated the change in S-parameter with positron-incident energies in 2/1 approximant crystal AlPdRu, and 1/0 approximant crystal AlPdRu. In the case of 1/0 approximant crystal, S-parameter increases from ~0 to ~ 1 keV. While, in the case of 2/1 approximant crystal AlPdRu, S-parameter increses remarkably from ~0 to ~0.5 keV. This means that the density of structural vacancies in 2/1 approximant crystal AlPdRu might be higher than that of 1/0 approximant crystal AlPdRu. These results are consistent with those of positron lifetimes of approximant crystals 2/1 AlPdRu and approximant crystals 1/0 AlPdRu by slow positron beams (unpublished data). Furthermore, the present results seem to be reasonable from the standpoint of the metallic-covalent bonding conversion which occurs according to the occupation and vacancy of the center sites of the Al icosahedral clusters. Unfortunately, we could not prepare the sample of AlPdRu quasicrystals. In order to investigate the relationship between structure, bonding nature, and electrical properties, in Al-based quasicrystals, positron annihilation measurements of AlPdRu quasicrystals have been required.

We have done the coincidence Doppler broadening spectra of 2/1 approximant crystal AlPdRu and 1/0 approximant crystal AlPdRu. To identify the positron trapping sites in 2/1 approximant crystal AlPdRu and 1/0 approximant crystal AlPdRu, the core electron momentum distribution of samples were measured by the coincidence Doppler broadening spectra. Experimental results suggest strongly that the trapping sites of 2/1 approximant crystal AlPdRu and 1/0 approximant crystal AlPdRu seem to be Similar.

REFERENCES:

[1] K. Kimura and S. Takeuchi in Quasicrystals: The State of the Art, 2nd ed., D.P. Divincenzo and P.J. Steinhart eds., World Scientific, Singapore (1999) pp.325-309.
[2] D. Mayou *et al.,* Phys. Rev. Lett. **70** (1993) 3915.
[3] K. Kimura *et al.,* J. Solid State Chem. **133** (1997) 302.
[4] K. Kirihara *et al.,* Phys. Rev. Lett. **85** (2000) 3468.
[5] I. Kanazawa *et al.,* Phys. Rev. Lett. **79** (1997) 2269.
[6] K. Yamada *et al.,* Philog. Mag. **98** (2018) 107.
[7] R. Tamura *et al.,* J. Phys:Condens. Matter **11** (1999) 10343.

CO4-18 Absorption Coefficient of Amino Acid in the Sub-THz region using CTR

T. Takahashi

Institute for Integrated Radiation and Nuclear Science, Kyoto University

INTRODUCTION: Coherent radiation emitted from a short bunch of relativistic electrons is useful as a bright light source in the THz-wave and millimeter wave regions for the spectroscopic purpose. Coherent transition radiation (CTR), which is emitted from a boundary between two media, is one of such a coherent light source. CTR is usually utilized as a non-polarized light source, because the electric vector of transition radiation (TR) emitted from a metallic screen is axially symmetric with respect to the trajectory of an electron beam. In this wavelength range, it is difficult to generate the circularly polarized light because of the property of the optical device. In my previous reports [1] the circularly polarized CTR using a pair of wire-grid radiators with the different polarization has been developed with a new idea. The significant point of my new technique is the use of linearly polarized CTR with the wire-grid radiator. With this technique the polarization degree is able to be controlled precisely. Circularly polarized light has been useful in the circular dichroism spectroscopy. Before using the light, spectra of some kinds of amino acid have been measured using linearly polarized CTR [2]. In this report absorption coefficients of them are compared.

EXPERIMENTAL PROCEDURES: The experiment was performed at the coherent radiation beamline [3] at the L-band linac of the Research Reactor Institute, Kyoto University. The energy, the width of the macro pulse, and the repetition rate of the electron beam were 42 MeV, 47 ns, and 60 Hz, respectively. The average current of the electron beam was 2.3 μA.

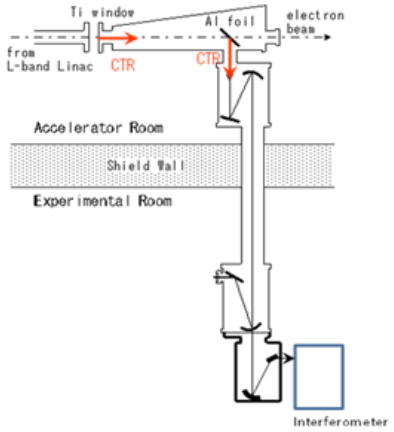

Fig.1 The schematic diagram of the experiment.

The spectrum of CTR was measured by a Martin-Puplett type inter- ferometer and a liquid-helium-cooled Si bolometer. The schematic diagram of the experiment was shown in Fig.1. Figure 2 is the photograph of the spectrometer and the detector.

RESULTS: The thickness of these samples was 2 mm. Calculated absorption coefficient of α -Alanine, Phenylalanine, and Tryptophan, are shown in Figs. 3. Difference between L and D forms has been observed. In order to investigate this discrepancy, it is necessary to measure using the circularly polarized light.

REFERENCES:

[1] T. Takahashi, *et al.*, KURRI-PR 2015 CO4-7.
[2] T. Takahashi, *et al.*, KURRI-PR 2016 CO4-8.
[3] T. Takahashi *et al.*, Rev. Sci. Instrum. **69** (1998) 3770.

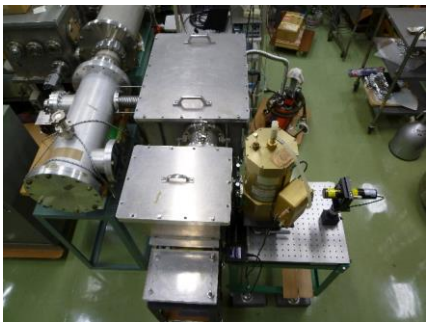

Fig.2 The photograph around the spectrometer.

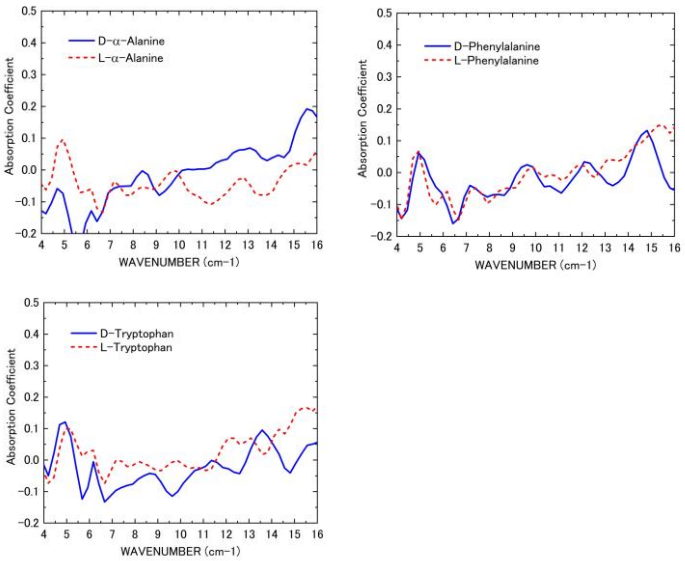

Fig.3 Absorption Coefficient of some kinds of amino acid.

CO4-19 Vacancy migration behavior in CoCrFeMnNi high entropy alloys and their subsystems

K. Sugita, M. Mizuno, A. Yabuuchi[1], A. Kinomura[1] and H. Araki
Graduate School of Engineering, Osaka University
[1]*Institute for Integrated Radiation and Nuclear Science, Kyoto University*

INTRODUCTION: Alloy design has traditionally been done by selecting the base material and adding the appropriate elements to achieve the desired properties. In the last decade, a new type of multicomponent alloy called "high entropy alloys" containing equiatomic / near-equiatomic ratios of constituent elements was proposed by Yeh et al [1-3]. These alloys often exhibit simple solid solution structures at high temperatures due to the high constituent entropy of random solid solution mixtures. High entropy alloys have been reported to have promising properties for practical use, such as high strength, high fracture toughness, excellent oxidation resistance and corrosion resistance combined with ductility. A major factor in these properties is thought to be the kinetics of "sluggish diffusion". Therefore, the diffusion kinetics of high entropy alloys has been actively studied by diffusion logarithms and tracer diffusion methods, as the atomic diffusion in a multiprincipal element matrix has also been of interest. In this work, we contribute to a debate about hypothetical sluggish diffusion phenomena in high entropy alloys by investigating the vacancy migration behavior in CoCrFeMnNi high entropy alloys and their subsystems during the isochronal annealing after electron-irradiation.

EXPERIMENTS: Vacuum induction melted ingots of CoCrFeMnNi, $CoCrFe_{0.25}MnNi$, CoCrFeNi and CrFeNi alloys were purchased from Koujundo chemical laboratory (Japan). The ingots were homogenized at 1373K for 24 h in silica tubes under Ar atmosphere, and were then machined into 10 × 10 × 0.5 mm plate pieces by electric discharge machining. The alloy ingots were cut into square plate specimens with dimensions of 10 × 10 × 0.5 mm^3. The specimens were subjected to strain relief annealing at 1373K for 10 h and then rapidly cooled to prevent secondary phase precipitation and to stabilize single-phase FCC structures. The specimens in water flow were exposed to 8 MeV electron beam irradiation for 3 h in KURNS-LINAC. The irradiation damage was evaluated at (1.3 - 1.8) $\times 10^{-4}$ dpa. In order to investigate the thermal stability of vacancies, the electron irradiated specimens were subjected to the subsequent isochronal annealing at 373-673 K for 1 h.
Positron lifetime measurements were carried out by using a digital oscilloscope system with photomultiplier tubes mounted with BaF_2 scintillators, having a time resolution (FWHM) of 180 ps. The positron lifetime measurements require data acquisition for approximately 15 hours with a Na-22 positron source of 0.5 MBq activity in order to acquire 3 million counts in the positron lifetime spectrum. The measured spectra were analyzed using the programs RESOLUTION and POSITRONFIT Extended.

RESULTS: The mean positron lifetime after isochronal annealing of the electron irradiated samples is shown in Fig.1. The positron lifetime spectra of as-irradiated samples show a clear separation into two exponential components of positrons with a long lifetime of 185-195 ps. This indicates that a part of positrons is trapped by monovacancies or relatively small vacancy clusters introduced by during the electron irradiation. After the subsequent isochronal annealing, the mean positron lifetime is found to decrease sharply around 473K. This can be attributed to the decrease in vacancy concentrations triggered by the free vacancy-migration. It demonstrates the vacancy migration enthalpy in the CoCrFeMnNi high entropy alloy is very similar to that in the CrFeNi alloy. These results indicate that the "'sluggish diffusion" hypothesis is not supported in CoCrFeMnNi high entropy alloys and their subsystems at least in view of vacancy migration behavior.

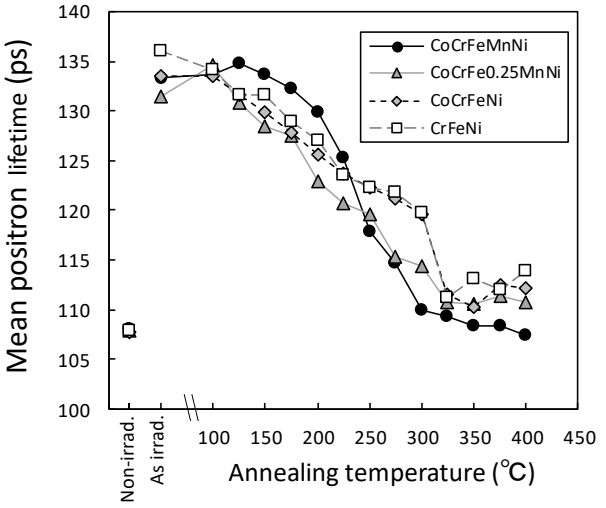

Fig. 1 Mean positron lifetime in the electron-irradiated CoCrFeMnNi, $CoCrFe_{0.25}MnNi$, CoCrFeNi and CrFeNi alloys after isochronal annealing.

REFERENCES:
[1] C. Y. Hsu, J. W. Yeh, S. K. Chen and T. T. Shun, Metall. Mater. Trans., **35A**(2004), 1465.
[2] J. W. Yeh, S. K. Chen, S. J. Lin, J. Y. Gan, T. S. Chin, T. T. Shun, C. H. Tsau and S. Y. Chang, Adv. Eng. Mater., **6** (2004). 299.
[3] J. W. Yeh, Ann. Chim. Sci. Mat., **31** (2006), 633.

CO4-20 Observation of Gamma-ray Induced Current on Coaxial Cable for Analog Data Transfer

Y. Gotoh, Y. Okuno[1], N. Sato[2], M. Imaizumi[3], T. Kobayashi[4], M. Akiyoshi[5], and T. Okamoto[6]

Graduate School of Engineering, Kyoto University
[1]Nuclear Science and Engineering Center, Japan Atomic Energy Agency
[2]Institute for Integrated Radiation and Nuclear Science, Kyoto University
[3]Research and Development Directorate, Japan Aerospace Exploration Agency
[4]Center for Advanced Photonics, RIKEN
[5]Radiation Research Center, Osaka Prefecture University
[6]National Institute of Technology, Kisarazu College

INTRODUCTION: In nuclear decommissioning of Fukushima Daiichi Nuclear Power Plant, observation of the inside of the primary containment vessel (PCV) is one of the key issues. For this purpose, many sensors including image sensor and radiation sensor have been under development [1, 2]. The data transfer from these devices put into the PCV should be made by cable, because radio wave cannot propagate out. The cable is also exposed to the radiation field, and therefore some currents would be induced by radiation. Such currents may cause an error in the sensor output. Therefore, it is important to know how large current would be induced at the cable, and to suppress the generation of the current. For this purpose, we have observed the current induced at a coaxial cable by gamma-ray irradiation.

EXPERIMENTS: The gamma-ray irradiation was performed at Co-60 gamma-ray irradiation facility at Institute for Integrated Radiation and Nuclear Science, Kyoto University. The coaxial cable examined in this study was 1.5D-QEV. A 15 m-long 1.5D-QEV cable was wound with a diameter of 20 cm. One end of the cable was connected to a coaxial cable of RG58A/U, which had been lain for taking the signal out of the irradiation room. The measurements of the current were performed with a compact pico-ammeter. Another end of the cable was terminated with a silicon diode installed in stainless steel can equipped with the connector of the coaxial cable. Use of the silicon diode was because it has similar structure with the solar cells, but it generates photocurrent only a little. For comparison, measurements were done with the cable with the end open. For both cases, the outer shield was grounded. Measurements were also made without grounding the outer shield of the cable. The cable was set at the position with different distance from the gamma-ray source. It was not easy to estimate the dose of irradiation to the cable accurately, the results were arranged with the dose rate at the center of the wound cable; the practical dose rate would be lower than this value.

RESULTS: Figure 1 shows the results of the observed currents as a function of the dose rate at the center of the wound cable. The data in Fig. 1 were acquired with the grounded cable. When the one end of the cable was open, approximately -40 pA was observed at the position where the dose rate of irradiation was 200 Gy/h. When the end was terminated by a silicon diode, the current increased to about -110 pA at the same position. If the difference of these results was attributed to the generation of photocurrent of the diode including radiation excited one, the current should be shift towards positive. The reason for the difference has not yet been clarified. The slope at the lower dose rate region is steeper than that at the higher dose rate, and this would be attributed to the fact that the actual dose rate was lower than that at the center of the wound cable.

When the outer shield of the cable was not grounded, the observed currents showed positive value in most cases. It was also shown that the observed current had a gradual change. These phenomena would be due to the charging of the cable. The present study showed the fact that grounding the outer shield of the cable is important not only for the cancelling the electric noise but also for suppressing the radiation effects.

ACKNOWLEDGEMENTS: The present study was supported by "Development of Dosimeter in Harsh Core Radiation Environment", through the Center of World Intelligence Project for Nuclear S&T and Human Resource Development by Japan Atomic Energy Agency.

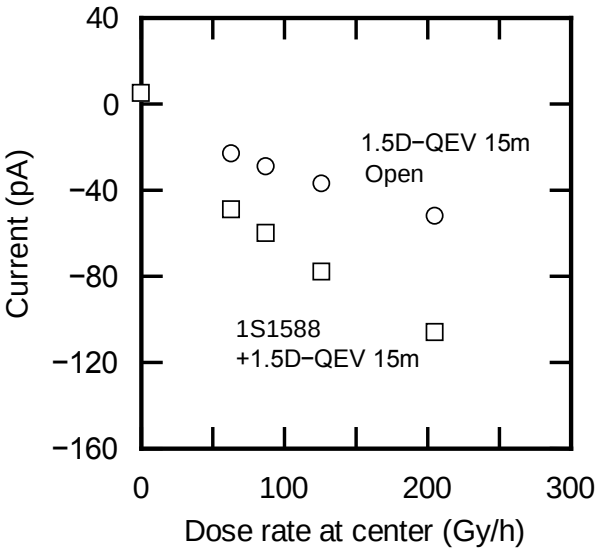

Fig. 1. Observed currents of the 1.5D-QEV cables under the gamma-ray irradiation.

REFERENCES:

[1] Y. Gotoh *et al.*, IEEE Trans. ED **67** (2020) 1660-1665.
[2] T. Okamoto *et al.*, "Development of Dosimeter in Harsh Core Radiation Environment", Workshop on Multicomponent Compounds and Solar Cells, Tokyo, November 30 – December 1, 2018.

CO4-21 Correlation between Damage Accumulation by Neutron Irradiation and Hydrogen isotope Retention for Plasma Facing Materials

Y. Oya, M. Nakata, A. Koike, S. Yamazaki, T. Wada, M. Zhao[1], F. Sun[2], Q. Xu[3], Y. Iinuma[3] and R. Okumura[3]

Graduate School of Integrated Science and Technology, Shizuoka University
[1]Graduate School of Science and Technology, Shizuoka University
[2]Faculty of Science, Shizuoka University
[3]Institute for Integrated Radiation and Nuclear Science, Kyoto University

INTRODUCTION: Due to the higher melting point and lower sputtering yield, tungsten (W) is considered as a candidate for plasma facing materials (PFMs) in the future fusion reactors. During the operation, W will be exposed to 14 MeV neutrons produced by D-T fusion reaction. The damages introduced by 14 MeV neutrons are considered to enhance hydrogen isotope retention compared to that for undamaged W. For the development of the effective fuel recycling and the safety operation, it is necessary to clarify the correlation between hydrogen isotope retention and damage level in W produced by neutron irradiation. In this study, irradiation damages were introduced by neutron and damage level was controlled by irradiation time, and the D retention behaviors were evaluated by thermal desorption spectroscopy (TDS). To evaluate the damage level by neutron irradiation, positron annihilation spectroscopy (PAS) was also performed.

EXPERIMENTS: A disk-type polycrystalline W (6 mm^{φ}×0.5 mm^{t}) purchased from A.L.M.T. Co. Ltd. was used. To remove impurities and damages introduced during the polishing processes, the samples were heat-treated at 1173 K under ultrahigh vacuum (< 10^{-6} Pa). Thereafter, the samples were damaged with damage concentrations up to 4.6×10^{-6} – 4.6×10^{-5} dpa (displacement per atom) by the fission neutron irradiations under 323 K in Kyoto University Research Reactor Institute (KUR) After the damage irradiation, the 1.0 keV deuterium ion (D_2^+) implantation was performed on the W sample at Shizuoka University. The D ion fluence was set to be 1.0×10^{22} D^+ m^{-2} with the ion flux of 1.0×10^{18} D^+ m^{-2} s^{-1}. The D desorption behavior was evaluated by TDS at the temperature up to 1173 K with the heating rate of 0.5 K s^{-1}.

RESULTS AND DISCUSSION: Fig. 1 shows D_2 TDS spectra for neutron damaged W samples and undamaged W sample. Positron lifetime of these samples are shown in Fig. 2. The D_2 TDS spectra were assumed to consist of four major D desorption stages located at 400 K, 550 K, 650 K and 850 K, respectively. Based on our previous studies, the D desorption stages were corresponded to the desorption of D adsorbed on the sample surface or trapped by dislocation loops, vacancies, vacancy clusters and voids, respectively [1]. In the neutron irradiated sample, D was adsorbed on the surface and/or trapped by dislocation loops and vacancies more than undamaged sample. Almost no D retention by vacancy clusters or voids were observed. These results were consistent with PAS results that long lifetime components which are considered as the existence of vacancy clusters or voids were not observed. In our previous report [1, 2, 3], the damages would suppress D diffusion according to the result of HIDT simulation. It was considered that the D diffusion was limited more for the sample irradiated up to damage level of 4.6×10^{-5} dpa than that of 4.6×10^{-6} dpa sample caused by the increase of vacancies by neutron irradiation. It was concluded D retention trapped by vacancies was increased with increasing the damage level.

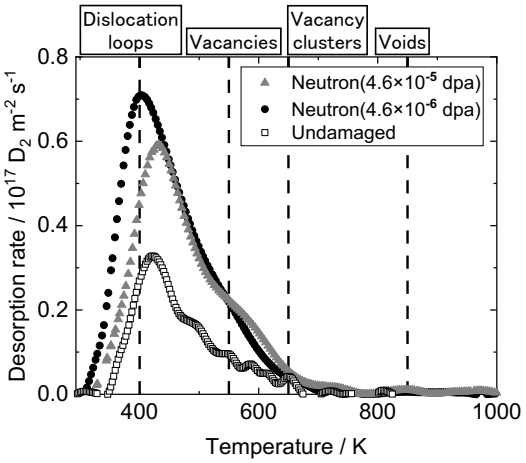

Fig. 1. D_2 spectra for neutron irradiated W and undamaged W.

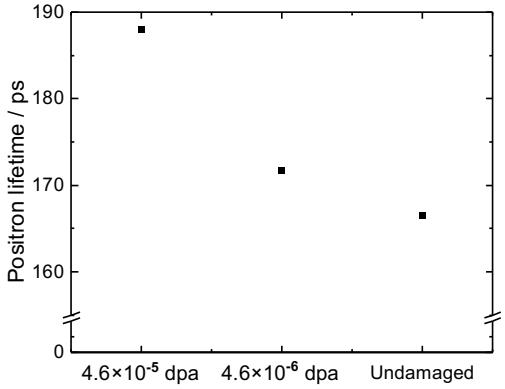

Fig. 2. Comparison of positron lifetime for neutron irradiated W and undamaged W.

REFERENCES:

[1] H. Fujita, K. Yuyama, X. Li, *et al:* Phys. Scr. **T167** (2016) 014068.
[2] M. Nakata, K. Azuma, A. Togari, *et al:* Fusion Engineering and Design, **Volume 146, Part B**(2019) 2096-2099.
[3] M. Nakata, A. Togari, F. Sun, *et al:* Fusion Science and Technology, Submitted.

CO4-22 Complex Structure of Ions Coordinated with Hydrophilic Polymer 20. Ionic Diffusion in Polymeric Structure Utilized by Polyiodide Ions. (1)

A. Kawaguchi and Y. Morimoto

Institute for Integrated Radiation and Nuclear Science, Kyoto University

INTRODUCTION:

We have been investigating dynamical and interacted structures between iodine (polyiodide ions, I_n^{m-}, *m, n*: integer, $n > 1$) and polymers.[1] While polyiodide ions (and their counter-ions, ex. K^+ ion which presented within I_2-KI(aq)) are prepared as solutes in aqueous solution, they can be diffused into various polymeric matrix without softening nor melting. Such structures and procedures are expected to introduce novel functionality and wide applications to modify polymeric materials with easy operation at R.T.[2]

Or, ionic diffusion of polyiodide ions and their counter ions from aqueous solution of polyiodides ("(1st) iodine doping") can advance not only into hydrophilic polymers, such as polyamide-6 (PA6) or polyvinyl-alcohol (PVA), but also into hydrophobic polymers, such as polyethylene (PE) or polyethylene-terephthalate (PET); polyiodide ions in the aqueous solutions can easily diffuse even into *hydrophobic* matrices without melting.[3] Or, within some hydrophilic matrix, modification of structure (orientation of polymer chain, intercalated structure,,) can be also observed.

Furthermore, posterior ionic diffusion on the previous presence of polyiodides ("secondary doping") can also advances for both hydrophilic polymers and hydrophobic ones as ionic exchange process with the counter-ion previously introduced in "(1st) iodine doping". As phenomena, iodine-doped polymers can be regarded as "pseudo solvents" for ionic diffusion.[4,5] Inner precipitation of inorganic fillers can introduce hybrid composites without melting nor softening process for matrix and, occasionally, can be applied for electroless plating on hydrophobic surface with aqueous solution.

Such unexpected behaviors of polymeric structures in existence of iodine (polyiodide ions) may be suggesting contradictive effects: activated diffusive environments (softening, plasticization, disordering in matrix,) vs. ordered structure (crystallization of crystalline polymer, precipitation of inorganic fillers, modified orientation of matrix).

On the other hand, structure of polyiodide ions can be also modified vaguely; they are able to change molecular structure and charge distribution not only in one molecule but between the polyiodide ions, cooperatively and interactively. Therefore, interactive dynamics and structure between polymers and iodine should be explained by extraordinary (also comprehensive and fundamental) schemes specified for polymeric structure and polyiodide ions.

DISCUSSION:

In the previously reported application utilizing "iodine doping" and following "secondary doping", the results mean activation of ionic diffusion in inner space of polymers. Characteristic and dynamic structure of the polyiodide ions show (almost general) affinity to both hydrophilic polymers and hydrophobic ones.

At first, we have to consider diffusion process of polyiodide ions into inner space of polymers, both for hydrophilic matrix and hydrophobic one while the polyiodide ions (and counter-ions) are solutes in aqueous solutions. Even though diameter of iodine atom is c.a. 4Å, they can be spontaneously diffused in polymeric matrix at room temperature; especially in some hydrophilic polymers (PA6, PVA,,), their diffusion is rapid and deep into the matrix. On the other hand, while iodine exist as mono-iodide ion (I^-) or tri-iodide ion (I_3^-) in each aqueous solution for "(1st) iodine doping" process, polyiodide ions doped and coordinated within polymers occasionally exist as I_3^- or tetra-iodide ion, I_5^-. It means that iodine elementally exists as polyiodide *ions* which have ionic charge and that counter ions (K^+, Na^+, NH_4^+, ,,) also exist simultaneously; they do not exist as "not-charged" molecules, such as methanol.

Secondly, polyiodide ions which are doped and exist at inner space of polymeric matrix is *not* ones as molecules in the aqueous solutions prepared on "iodine doping"; even if I_3^- molecules exist in deep region of the matrices, they are *not* the similar molecules solved as the solutes in the solution for "iodine doping". Or, it should be remarked that I_5^- which is occasionally observed in coordination with polymeric matrix is very minor components in each aqueous solutions on "iodine doping"; I_5^- molecules are not diffused from the solutions but *in situ* rearranged at inner space of matrix. It is not diffusion of unchanged molecules but diffusion of the molecules modified through diffusion. Since polyiodide ions can easily change their molecular structure and charge distribution, they can be diffuse as different structure from solute in the aqueous solutions and as efficient form for diffusion and binding. And it does not matter whether the coordinated form or molecular structure is different from the solutes in the doping solution or not. [to be continued]

ACKNOWLEDGMENTS: These results are researched with Dr. Gotoh (Shinshu Univ.) and his staff and are partially funded by NEDO.[6]

REFERENCES:

[1] A. Kawaguchi, Polymer, **35**, 3797-3798 (1994).

[2] patent. JPN-5444559 (2014).

[3] A. Kawaguchi, *et.al.,* KURRI Prog.Rep.2015, 79-79. (2016).

[4] A. Kawaguchi *et.al.,* SPring-8 User Exp. Rep. **5** (2000A), 354-354 (2000).

[5] A.Kawaguchi, Polym.Prep.Jpn., **62**,5116-5117 (2013).

[6] "Projects for Practical Use from Innovation" sponsored by NEDO (2007-2009).

CO4-23 A study on destruction of cesium aluminosilicate cage by gamma irradiation (1)

H. Ohashi, R. Takaku and T. Saito[1]

Faculty of Symbiotic Systems Science, Fukushima University

[1]*Institute for Integrated Radiation and Nuclear Science, Kyoto University*

INTRODUCTION: Pollucite which is one of cesium aluminosilicate com-pounds have attracted attention as a final storage mate-rial of ^{137}Cs. Pollucite is able to synthesized by hydro-thermal method in low temperature below 300°C [1]. Pollucite has various properties that favor the immobilization of Cs ions.

However, the damage to the aluminosilicate framework by radiation decay is concerned because it contains ^{137}Cs. It has been reported that the effect of β-ray emission and nuclide conversion by β-decay of ^{137}Cs on aluminosilicate framework is minor [2, 3]. On the other hand, there are few reports of effects by gamma rays on pollucite framework. Therefore, we examined the effect of gam-ma radiation on the aluminosilicate framework of Pollucite. Pollucite samples were synthesized to investigate the effect of gamma irradiation.

EXPERIMENTS: The solution was prepared at the Al concentration of 50 mmol L^{-1} and the composition ratio of Cs_5 Al_1 Si_2 O_6 Na_{10} $Cl_{11.2}$ K_2 $Ca_{0.2}$ $(OH^-)_{2.2}$ $(H_2O)_{220}$, and placed in a Teflon inner cylinder pressure container. Pollucite was synthesized by hydrothermal method, holding the container at 180 °C for 72 hours. The resulting precipitate was washed. Thereafter, each solid was collected by filtration and dried at 110 °C for 16 hours or more.

The powder sample was divided into four, three of which were gamma-irradiated at 1, 10, and 100 kGy. Characterization was performed by XRD. The 7 days leaching test by PCT-A method [4] was carried out to evaluate the change of Cs retention performance by framework damage. The normalized release rate, NRCs [g m^{-2} d^{-1}], was calculated by equation (1).

$$NR_{Cs} = \frac{C_{Cs}}{f_{Cs}\frac{SA}{V}t} \qquad (1)$$

Where C_{Cs} [g L^{-1}] was the concentration of Cs in the solution, f_{Cs} was the weight ratio of the Cs in the sample before leaching, SA [m^2] was the sample surface area, V [L] was the volume of the leaching liquid, and t [day] was the test duration.

RESULTS: Figure 1 shows the XRD patterns of Pollucite sample before and after gamma irradiation, and the diffraction peak of Pollucite was indicated by the Miller index. All the patterns showed that they contained only single-phase pollucite. None of gamma irradiation sample did not shifted diffraction peeks compared to before irradiation one. This indicated that there was no change in the crystal structure of Pollucite.

Table 1 shows the various parameters obtained by the leaching test according to the PCT-A method, and the normalized release rate (NR_{Cs}). In previous reports [5], the NR_{Cs} of Pollucite was around 10^{-5} to 10^{-6} [g m^{-2} d^{-1}], and was similar to the all samples after gamma irradiation at this study. This indicated NR_{Cs} was not increased by gamma irradiation.

From the above results, it was considered that the effect of gamma irradiation on the aluminosilicate framework of pollucite was not mostly observed until 100 kGy.

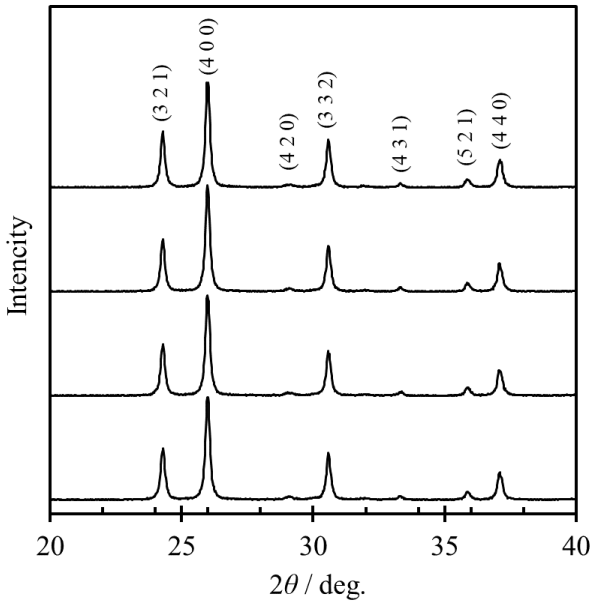

Fig.1. XRD patterns of (a) without irradiated, (b) 1 kGy, (c) 10 kGy, and (d)100 kGy irradiated sample.

Table 1. Leaching test parameters in this study.

Dose [kGy]	f_{Cs}	$SA\ V^{-1}$ [m^2 L^{-1}]	NR_{Cs}
without-irr.	0.35	134	1.5×10^{-4}
1	0.35	141	1.5×10^{-4}
10	0.35	141	1.2×10^{-4}
100	0.35	141	1.3×10^{-4}

REFERENCES:

[1] Y. Yokomori *et al.*, *Sci. Rep.*, **4** (2014) 4195.
[2] J. Fortner *et al*., Argonne National Laboratory, Argonne, Illinois 60439 (2001).
[3] N. J. Hess *et al.*, *J. Nucl. Mater.*, **281** (2000) 22-33.
[4] ASTM C 1285-02 (2008).
[5] Z. Jing *et al.*, *J. Hazard. Mater.*, **306** (2016) 220–229.

CO4-24 Effects of Buffers and Salts on Nanostructure of Soybean Proteins as Revealed by SAXS

N. Sato, R. Urade, A. Okuda, K. Morishima, R. Inoue, and M. Sugiyama

Institute for Integrated Radiation and Nuclear Science, Kyoto University

INTRODUCTION: It has long been known that soybeans contain abundant proteins. They consist of more than 30% of dry matters of their seed. Thus, soybeans have been eaten as nutritious natural food, not only as unprocessed beans but also as soybean food products such as *tofu* and *tofu* skin (*yuba*). *Tofu* is a kind of hydrogels composed of soybean proteins, and accordingly its property and quality are subject to coagulation behavior of soybean proteins. Aside from traditional soybean food products like *tofu*, soy protein isolate (SPI) have been industrially produced and provided to the commercial market in recent years for improving physical property of various food products by adding them to those foods. Soybean proteins are also used for making mimic meat products for vegetarians and vegans. World-wide increase in health consciousness leads to growing importance of soybean protein usage. From these reasons, soybean proteins are one of key substances in the field of food science.

In order to obtain high-quality soybean food products or SPI-containing foods, it is necessary to deeply understand the structure of soybean proteins at the molecular level. In particular, structural changes induced by the various conditions such as temperature change, salt addition and coagulant addition are of great significance to elucidate the relationship between the structure of proteins and the physical property of foods containing soybean proteins. For structural analysis on opaque, disorder and condensed soft matters such as gels, colloids, and rubber, small-angle X-ray and neutron scattering (SAXS, SANS) has been proved to be a useful technique, and it is also expected to be effective for structural analysis of foods, which has similar features to above soft matters. Therefore we have been studying the nanostructure of wheat and soybean proteins by SAXS and SANS. The behavior of isolated and aggregated protein molecules in aqueous solutions and hydrates has been investigated by taking advantage of SAXS and SANS.

In this study, we conducted a SAXS analysis on two major soybean proteins, β-conglycinin and glycinin, which have been conventionally referred to as 7S and 11S, respectively, according to their sedimentation coefficients determined by analytical ultracentrifugation. Difference of nanostructure of 7S and 11S in pure water and buffer solutions was examined by SAXS. Effects of NaCl addition was also investigated.

EXPERIMENTS: Soybean proteins 7S and 11S were extracted from hexane-defatted powder of soybean cultivar "Enrei" under a reducing condition with 2-mercaptoethanol. Isoelectric precipitation was applied to isolation of each protein. By adjusting pH of the extract solutions, 11S and 7S was precipitated at pH 5.8 and pH 4.5, respectively. SAXS measurements were performed with a laboratory SAXS instrument (NANOPIX, Rigaku) installed at Institute for Integrated Radiation and Nuclear Science, Kyoto University. Each protein dissolved in pure water or 35-mM potassium phosphate (KPi) buffer solutions at pH 7.5 in presence of 0 or 0.8 M NaCl was put into aluminum cells and set for SAXS measurements. The wavelength of X-ray was 1.54 Å, the sample-to-detector distance was 1300 mm and the available q-range was 0.08 – 2.2 nm^{-1}. Model calculation of SAXS profiles from crystal structure was done with a software, CRYSOL [1].

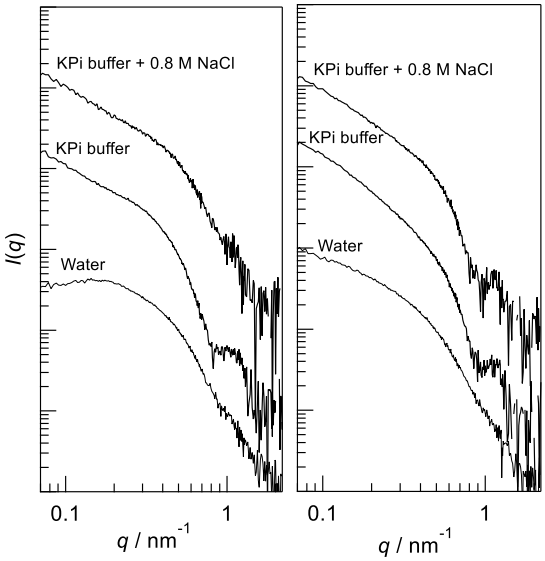

Fig. 1 SAXS profiles for 7S (left) and 11S (right) in 0.5% pure water and KPi buffer solutions.

RESULTS: Fig. 1 shows SAXS profiles measured for 0.5% 7S and 11S solutions at 25°C. A small peak appeared around 1.2 nm^{-1} in KPi buffer solutions, which is an indication of trimer ring structure consisting of three subunits. In pure water, however, this peak was not recognizable, suggesting that the subunits cannot form trimer ring structure and exist as monomers in pure water. When 0.8 M NaCl was added to the KPi solution of 7S, the peak at 1.2 nm^{-1} became weaker and the shoulder at 0.4 nm^{-1} shifted to higher-q. However, such changes were not observed for 11S. These profiles agree with the model calculation results for crystal structure of monomer, trimer and hexamer. Therefore it was demonstrated that monomeric subunits in pure water are assembled into hexamers in KPi buffer solutions by stacking two ring trimers, and dissociated into trimers at higher ionic strength conditions only for 7S.

REFERENCES:

[1] D.I. Svergun *et al., J. Appl. Cryst.,* **28** (1995) 768.

CO4-25 Porosity Measurements of Sintered-Silver Bonding Plates

K. Wakamoto, T. Otsuka, K. Nakahara, A. Yabuuchi[1] and A. Kinomura[1]

Power Device R&D Department, ROHM Co., Ltd.
[1]Institute for Integrated Radiation and Nuclear Science, Kyoto University

INTRODUCTION: Sintered silver has attracted much attention as a die-attach material for the power electronics, owing to its high heat dissipation capability [1]. On the other hand, the coefficient of thermal expansion (CTE) inevitably does not match each other of the materials used in a power system. Thus the heat-cycle oriented mechanical stresses deteriorate die-attach materials, and therefore the mechanical properties of sintered silver impinge on the reliability of electricity systems.

However, nobody can predict how long sintered silver sustains, because the material is porous and its mechanical properties heavily depends how porous it is. Accordingly, the research is highly demanded to measure the porosity.

The porosity rate (p) of sintered silver is reported by some papers [2-3], where p is measured by using cross sectional scanning electron microscopy (SEM). These studies focus only estimates the μm-order pores of sintered silver materials, not nm-order pores such as crystalline defects. Positron lifetime measurement method has advantages for this purpose. To this end, therefore, the authors used a conventional positron annihilation lifetime spectrometer in Kyoto University to estimate the nm-order pore sizes embedded in sintered silver with various p's by measuring the positron lifetime of the material.

EXPERIMENTS: The fabrication process of sintered silver films is described as follows. Paste including silver nm-particles was stencil printed on a metal plate, and the containing organic solvent was dried at 140ºC for 1 h. These dried films were sintered at 300 ºC for 10 min with uniaxial press via a carbon buffer sheet with 0.5 – 120 MPa pressure. The film shape was 5 mm square and 50-μm thick. Positron annihilation lifetime spectroscopy was performed to evaluate bulk lifetimes of the samples by using a ^{22}Na source sealed with 12.5 μm Kapton foils. The thickness of the samples was approximately 50 μm. Four sample plates were stacked and measured together to stop all the positrons from the source inside the sample. The measure samples are summarized in Table I.

Table I Summary of the measured specimens.

Sample	Sintering temp. (ºC)	Pressure (MPa)	Sample size
A	300	120	5mm square and 200-μm thick
B		80	
C		30	
D		0.5	

The spectrometer consists of two scintillation gamma-ray detectors with BF_2 crystals and a spectrometer based on digital circuits. Total counts for each measurement were approximately 10^6 counts.

RESULTS: The data from the 1st sample set to investigate pressure dependence was analyzed as follows. Measured lifetime spectra were decomposed into three components as shown in Fig. 1. The lifetimes and intensities of the first and third components changed depending on formation pressure, while the second lifetime and intensity were almost constant except for the lowest pressure sample. In fig. 1(a), average lifetimes calculated from lifetime and intensity values were plotted as well. The average lifetimes were almost constant for all the samples. The lifetime values obtained from a literature for bulk Ag and monovacancy in Ag were indicated with broken lines in fig. 1(a). The second and third lifetime components can be attributed to monovacancies and vacancy clusters. It is necessary to further investigate the origin of each lifetime components to know the behavior of nanometer-sized voids (vacancies) that cannot be detected in secondary electron microscopy.

SUMMARY: Porosity of sintered Ag plates was characterized as a function of formation pressure by conventional positron annihilation lifetime spectroscopy. The third lifetimes corresponding to vacancy clusters changed depending on formation pressure, while the average lifetime was almost constant.

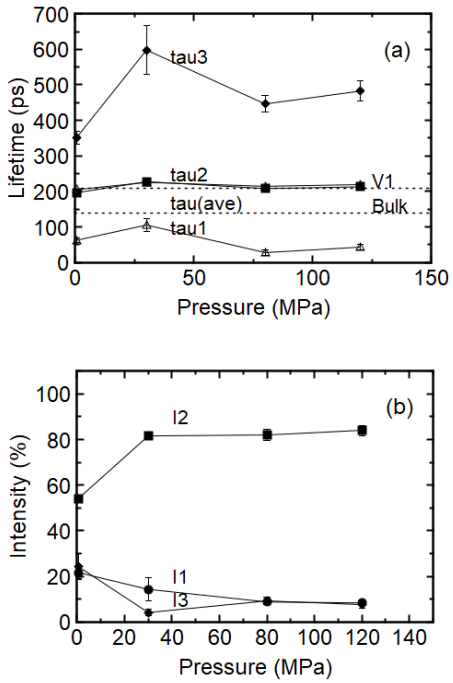

Fig. 1 Lifetimes and their intensities of the samples.

REFERENCES:

[1] KIM S. SIOW, Journal of ELECTRONIC MATERIALS., **43** (2014) 947-961.
[2] T. Yousseff *et al*., Microelectronics Reliability., **55** (2015) 1997-2002.
[3] M. Takesue *et al*., Proc. PCIM., (2018) 148.

CO4-26 Differences in the Recovery Behavior of Electron-Irradiation-Induced Vacancies in Metals with Different Purities

A. Yabuuchi, M. Tanaka, and A. Kinomura

Institute for Integrated Radiation and Nuclear Science, Kyoto University

INTRODUCTION: Since tungsten (W) is expected as a plasma-facing material for fusion reactors, many studies on vacancy-type defects in W are carried out using positron annihilation spectroscopy. Based on several first-principles calculations, the positron lifetime of monovacancy in W is expected to be 193−200 ps. On the other hand, defects having positron lifetimes of 165−180 ps have been observed in electron-irradiated W. In this study, the annealing behaviors of electron-irradiation-induced vacancies in two kinds of W samples with different purities were observed by using a positron annihilation lifetime spectroscopy in order to understand the cause of the difference between the calculated and experimental values. In addition, positron lifetimes in vacancy-impurity complexes consisting of several possible impurity atoms were also calculated and compared with experimental values.

EXPERIMENTS: Well annealed W samples having purities of 99.999% (5N) or 99.9% (3N) were irradiated with 8-MeV-electrons to a total dose of 5×10^{19} e^-/cm^2. The sample temperature was kept at about 373 K during the irradiation. The irradiated samples were isochronally annealed at 50 K steps with a duration of 15 min. After each annealing, positron annihilation lifetime measurements were performed at room temperature. The acquired positron annihilation lifetime spectra were decomposed into two components. The longer lifetime component was recognized as the component derived from the irradiation-induced vacancies.

RESULTS: Figure 1 shows the changes in the longer positron lifetimes and their intensities of both samples during isochronal annealing [1]. The positron lifetimes of both as-irradiated samples (~170 ps) are about 25 ps shorter than the calculated positron lifetime of isolated monovacancy (195 ps). This implies that the vacancies introduced into W by electron-irradiation does not exist as isolated monovacancies, but rather exist as vacancy-impurity complexes. The positron lifetime calculations revealed that the positron lifetime becomes shortened from 195 ps to ~170 ps when a monovacancy binds with interstitial-type impurity atoms such as carbon, oxygen, and nitrogen. It was also found that the positron lifetime of vacancy-hydrogen complex becomes only shortened to 185 ps, whereas it becomes shortened to ~170 ps when two hydrogen atoms are bound to a monovacancy.

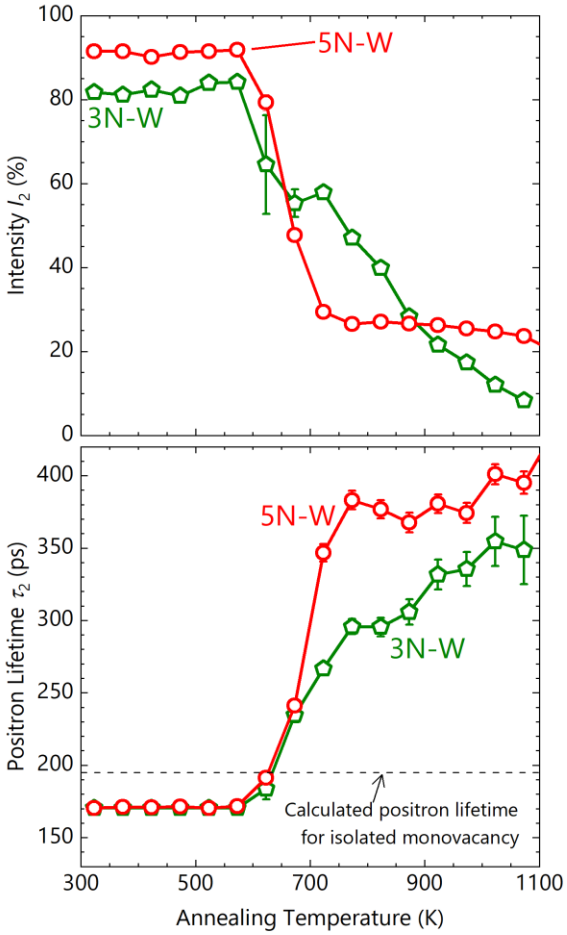

Fig. 1. Defect-related positron lifetimes τ_2 and their intensities I_2 for 5N- (open circles) and 3N-W (open pentagons) samples as a function of annealing temperature. Calculated positron lifetime for isolated monovacancy (195 ps) is also depicted as a dashed line.

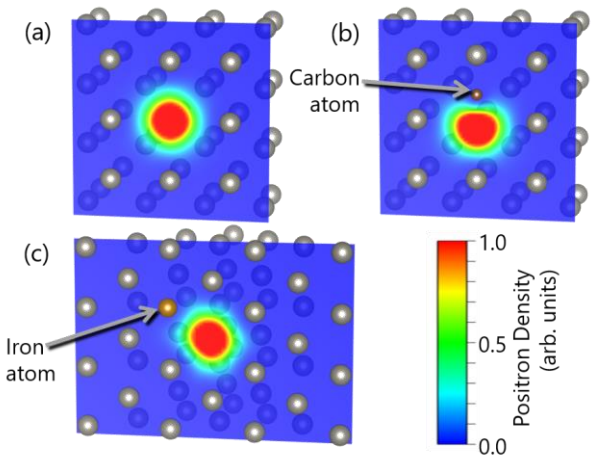

Fig. 2. Calculated positron density distributions at (a) isolated monovacancy, (b) vacancy-carbon complex, and (c) vacancy-iron complex. The atomic positions are also depicted as spheres.

REFERENCE:
[1] M. Tanaka, A. Yabuuchi, and A. Kinomura, AIP Conf. Proc., **2182** (2019) 050014-1−050014-4.

CO4-27 Differences in the Development of Vacancy-Type Defects During Annealing with Different Irradiated Ion Species

A. Yabuuchi, M. Tanaka, and A. Kinomura

Institute for Integrated Radiation and Nuclear Science, Kyoto University

INTRODUCTION: Since tungsten (W) is expected to use as a plasma-facing material for fusion reactors, the effects of hydrogen (H) and/or helium (He) ion irradiation into W have been well studied. Recently, several studies are carried out to reduce the heat load on W wall by injecting neon (Ne) or argon (Ar) gas into the fusion plasma. Positron annihilation spectroscopy is a useful tool for characterizing vacancy-type defects in materials. Thus, several positron-based studies of defects in H^+- or He^+-irradiated W have been reported. However, few studies have investigated the defects in Ne^+- and/or Ar^+-irradiated W by using positrons. Irradiating heavier ions than H^+ and/or He^+ may cause more serious damage to W. In this study, He^+- and Ne^+-irradiated W samples were prepared and investigated the differences in the developmental process of irradiation-induced defects during annealing by using a slow positron beam.

EXPERIMENTS: The well annealed W samples were irradiated with He^+ or Ne^+ ions with an energy of 50 keV. The irradiated and unirradiated samples were probed by a slow positron beam to acquire the Doppler broadening of the annihilation radiation (DBAR) spectra. The DBAR spectra were characterized by an *S*-parameter which represents the proportion of annihilation events with a small Doppler shift, and a *W*-parameter which represents the proportion of annihilation events with a large Doppler shift. In addition, *R*-parameters were also derived from the *S*- and *W*-parameters [1]. The *S*- and *W*-parameters depend on both defect species (defect size) and defect concentration, while the *R*-parameter does not depend on the defect concentration but only on the defect species.

RESULTS: Figure 1 shows the annealing temperature dependence of *S*-parameters for both irradiated samples. The increased *S*-parameters of as-irradiated both samples are finally reduced to the almost unirradiated-state by annealing at 900°C. Judging from the changes in *S*-parameters, superficially, the irradiation-induced defects appear to have been recovered in both samples. However, the changes in *R*-parameters shown in Fig. 2 indicate that the developmental processes of irradiation-induced defects in both samples are different during annealing. Figure 2 shows that defect species in the He^+-irradiated W finally become the same as those in the unirradiated W (*i.e.*, the irradiation-induced vacancies are fully recovered). In contrast, the changes in *S*-, *W*-, and *R*-parameters during annealing indicate that irradiation-induced vacancies aggregate and grow into larger vacancy clusters in Ne^+-irradiated W [2].

REFERENCES:

[1] S. Mantl and W. Triftshäuser, Phys. Rev. Lett., **34** (1975) 1554−1557.

[2] A. Yabuuchi, M. Tanaka, and A. Kinomura, J. Nucl. Mater. **531** (2020) 152018-1−152018-5.

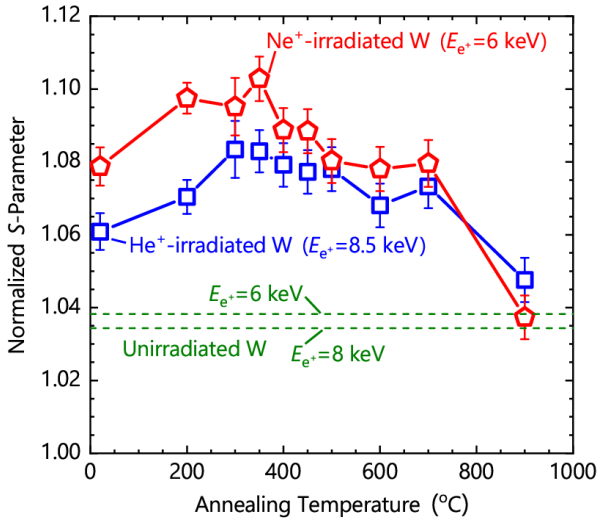

Fig. 1. *S*-parameters as a function of annealing temperature obtained from He^+- and Ne^+-irradiated tungsten. All the *S*-parameters are normalized to that obtained from unirradiated tungsten probed with positron energy of 20 keV. The He^+- and Ne^+-irradiated tungsten were probed with positron energies of 8.5 keV and 6 keV, respectively. *S*-parameters obtained from the unirradiated tungsten probed with positron energies of 6 keV and 8 keV are also depicted as dashed lines.

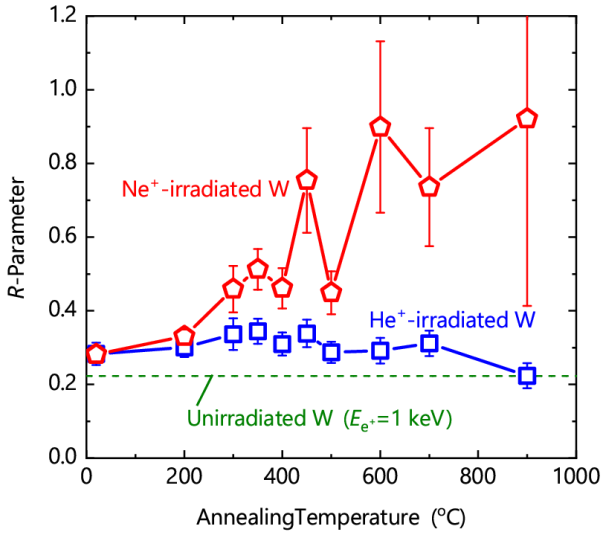

Fig. 2. *R*-parameters as a function of annealing temperature obtained from He^+-and Ne^+-irradiated tungsten. All the *R*-parameters are derived from the normalized *S*- and *W*-parameters. The *R*-parameter obtained from unirradiated tungsten probed with positron energy of 1 keV, corresponding to positron annihilation at the surface, is also depicted as a dashed line.

CO4-28 Defect Characterization of Ion-Irradiated $GdBa_2Cu_3O_{7-\delta}$ Superconducting Tapes Probed by a Slow Positron Beam

T. Ozaki, H. Sakane[1], T. Kashiwabara, A. Yabuuchi[2] and A. Kinomura[2]

School of Science and Technology, Kwansei Gakuin University
[1]SHI-ATEX Co., Ltd.
[2]Institute for Integrated Radiation and Nuclear Science, Kyoto University

INTRODUCTION: Superconducting materials, such as $GdBa_2Cu_3O_{7-\delta}$ (GdBCO) investigated in this work, are known to improve a high magnetic field resistance by forming lattice defects using ion-irradiation techniques. The Doppler broadening of annihilation radiation (DBAR) spectra become sharpened by annihilating positrons at vacancy-type defects, which enables us to characterize the concentration and/or size of vacancy-type defects [1]. In this work, tape-shaped GdBCO films irradiated with 2-MeV-Au^{2+} or 10-MeV-Au^{4+} ions were probed by a slow positron beam.

EXPERIMENTS: The GdBCO(500 nm)/CeO_2(150 nm)/Y_2O_3(150 nm)/Ni/Cu/SUS samples were irradiated with 2-MeV-Au^{2+} (4×10^{12} Au^{2+}/cm^2) or 10-MeV-Au^{4+} (6×10^{12} Au^{4+}/cm^2) ions. The 2 MeV and 10 MeV ions stop in the GdBCO film and penetrate the GdBCO film, respectively. The unirradiated and irradiated samples were probed by the KUR slow positron beam and the DBAR spectra were acquired. The sharpness of the DBAR spectra is evaluated by a value called the S parameter, which becomes generally lower when positrons annihilate in a perfect lattice, and higher when positrons are trapped into vacancies [1].

RESULTS: Figure 1 shows S parameters for the unirradiated sample as a function of incident positron energy. The S parameters in the energy region of 5−12 keV correspond to positron annihilation in the GdBCO film. Figures 2 and 3 show S parameters for the 2-MeV-Au^{2+}- and 10-MeV-Au^{4+}-irradiated samples. Contrary to our initial expectation, both irradiated samples show a reduction in S parameters compared to the unirradiated one. This reduction in S parameters implies that the unirradiated sample already contained vacancy clusters larger than irradiation-induced vacancies. When a large number of relatively small vacancies are formed by ion irradiation, most positrons are trapped at the irradiation-induced vacancies rather than the pre-existing vacancy clusters. Positrons annihilated in small vacancies bring smaller S parameters than positrons annihilated in vacancy clusters, and thus the reduction in S parameters was considered to be caused by ion irradiation.

REFERENCE:
[1] R. W. Siegel, Ann. Rev. Mater. Sci., 10 (1980) 393−425.

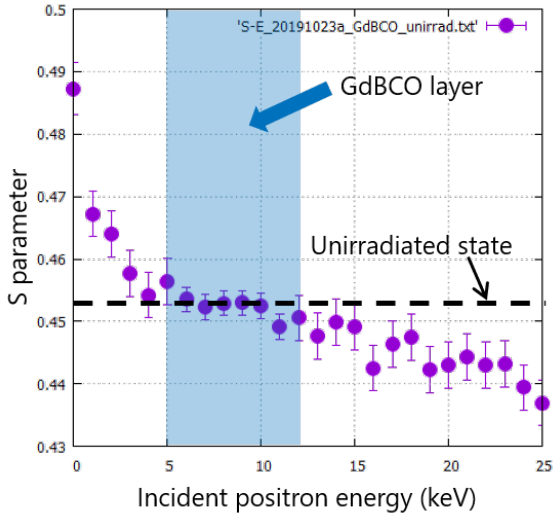

Fig. 1. *S* parameters for unirradiated GdBCO tape.

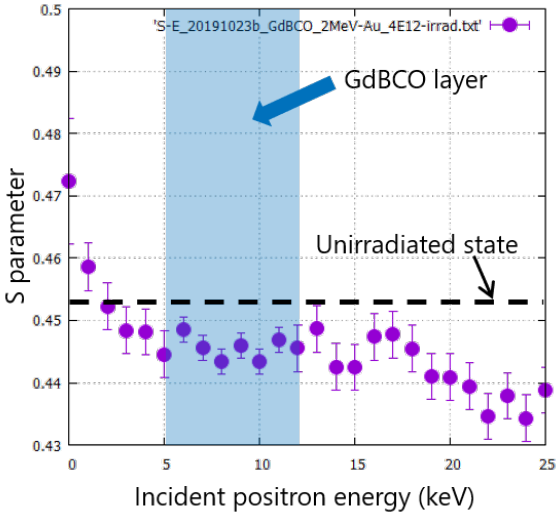

Fig. 2. *S* parameters for 2-MeV-Au^{2+}-irradiated GdBCO tape with a total dose of 4×10^{12} Au^{2+}/cm^2.

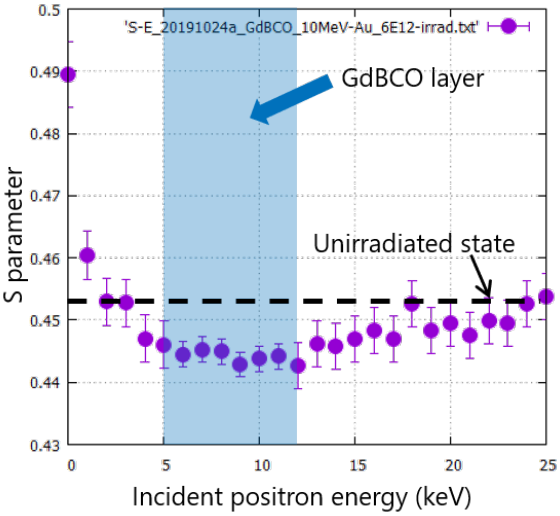

Fig. 3. *S* parameters for 10-MeV-Au^{4+}-irradiated GdBCO tape with a total dose of 6×10^{12} Au^{4+}/cm^2.

Neutron irradiation tests for ITER plasma diagnostics

M. Ishikawa, E. Yatsuka, R. Imazawa, T. Ushiki, H. Murakami and T. Hatae

National Institutes for Quantum and Radiological Science and Technology

INTRODUCTION: International Thermonuclear Experimental Reactor (ITER) [1] is being built in France by international cooperation. This study focuses on neutron irradiation effects on optical elements and piezo-actuators used in ITER. Expected 1 MeV Silicon equivalent fluence is 10^{12}-10^{15} n/c m^2 depending on locations of components. In order to investigate the effect of such high fluence on the actual components in a short time, neutron irradiation was performed using the slant exposure tube and the pneumatic tubes of the KUR. Although there are similar studies in Europe [2], they don't cover all the components necessary for ITER plasma diagnostic systems developed by Japan. This report mainly presents effect of neutron irradiation on optical components for Edge Thomson scattering (ETS) system. We conducted a neutron irradiation test on radiation-resistant glasses that are guaranteed to withstand gamma irradiation of 10 MGy. In addition, the tests for other systems such as the Poloidal Polarimeter and Infrared Thermography systems are briefly described.

EXPERIMENTS: Three kinds of radiation resistant glasses (BK7G18, LF5G19 and SF6G05) with anti-reflection coatings, products of Schott in Germany, were irradiated with neutrons. By using one of these glasses together with fused silica, chromatic aberration of the collection optics the ETS is compensated [3]. The glass samples in this study have diameter of 25 mm and thickness of 5 mm. These glasses were irradiated at the bottom of slant exposure tube for maximum 20 hours at 1-MW reactor output power. Fast and total neutron fluences were 6×10^{15} cm^{-2} and 6×10^{16} cm^{-2}, respectively, considering neutron spectra at slant exposure tube. Spectral transmissions of glasses before and after irradiation were measured with spectrophotometer (Hitachi U-2910) and compared.

RESULTS: Figure 1 shows photographs of radiation hard glasses (a) BK7G18, (b) LF5G19 and (c) SF6G05, respectively, before and after irradiation. The values in figure denotes fast neutron fluence onto each sample. Degradations on light transmission of BK7G18 and LF5G19 were clearly observed with visual inspection. Figure 2 shows the spectral transmissions of (a) BK7G18, (b) LF5G19 and (c)SF6G05, respectively. In the ETS, light within spectral range of 590-1070 nm is analyzed for electron temperature and density measurements in ITER. Before irradiation, LF5G19 had the highest spectral transmission in the range of 590-1070 nm. It was clarified that SF6G05 is the most insensitive to neutron irradiation in that spectral range. In contrast to the samples with thickness of 5 mm were tested, ETS is expected to be designed to use thicker (20-50 mm) radiation hard glass. That is, in reality, it is considered that the influence of the degradation of transmission will be more remarkable. Regarding SF6G05, drop of transmission around 800 nm (in total 4.3%) is mostly caused by reflections on surfaces (3.8%) rather than internal absorption (0.5%). If the antireflection coating is optimized, the initial transmittance may be improved to the same level as that of other types of glass. At present, SF6G05 seems promising as a glass for chromatic aberration compensation of ETS signal light under the neutron environment of ITER.

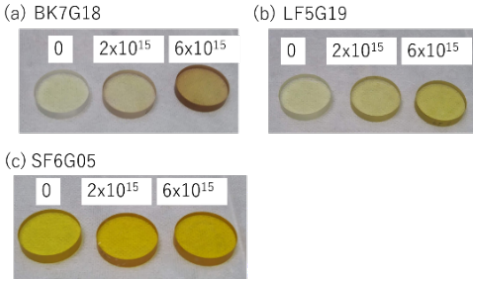

Fig. 1: Photographs of radiation hard glasses before and after irradiation.

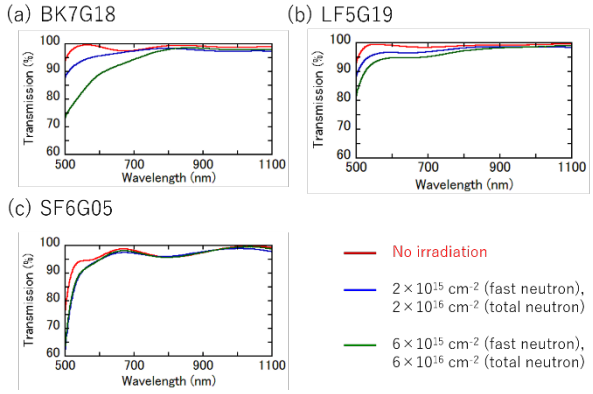

Fig. 2: Spectral transmissions of radiation hard glasses before and after irradiation.

ON GOING INVESTIGATIONS AND PROSPECTS:

Poloidal Polarimeter will be installed in ITER for measuring plasma current profile and use piezo actuators in radiological environment for adjusting laser beam position. Irradiation test of the piezo actuator was started from 2019. Target neutron fluence for the test is $9\text{x}10^{15}$ cm^{-2}. Functional tests after neutron irradiation are planned on 2020.

Infrared Thermography system will use coating mirror and lens in radiological environment. Irradiation tests of several candidate materials for mirror and lens were started from 2019. In 2020, the irradiation tests will be continued to investigate threshold value of total dose for keeping their optical performance.

REFERENCES:

[1] B. Bigot, Fusion Eng. Des., **146**, 124 (2019).
[2] M. Decreton *et al.*, J. Nucl. Mat., **329** Part A, 125 (2004).
[3] E. Yatsuka *et al.*, Fusion Eng. Des., **136**, 1068 (2018).